© 2020. Published by The Company of Biologists Ltd | Journal of Cell Science (2020) 133, jcs247684. doi:10.1242/jcs.247684

RESEARCH ARTICLE

Cargo-mediated recruitment of the endocytic adaptor protein Sla1 in *S. cerevisiae*

Thomas O. Tolsma, Hallie P. Febvre, Deanna M. Olson and Santiago M. Di Pietro*

ABSTRACT

Endocytosis of plasma membrane proteins is mediated by their interaction with adaptor proteins. Conversely, emerging evidence suggests that adaptor protein recruitment to the plasma membrane may depend on binding to endocytic cargo. To test this idea, we analyzed the yeast adaptor protein Sla1, which binds membrane proteins harboring the endocytic signal NPFxD via the Sla1 SHD1 domain. Consistently, SHD1 domain point mutations that disrupted NPFxD binding caused a proportional reduction in Sla1–GFP recruitment to endocytic sites. Furthermore, simultaneous SHD1 domain point mutation and deletion of the C-terminal LxxQxTG repeat (SR) region linking Sla1 to coat proteins Pan1 and End3 resulted in total loss of Sla1–GFP recruitment to the plasma membrane. These data suggest that multiple interactions are needed for recruitment of Sla1 to the membrane. Interestingly, a Sla1 fragment containing just the third SH3 domain, which binds ubiquitin, and the SHD1 domain displayed broad surface localization, suggesting plasma membrane recruitment is mediated by interaction with both NPFxD-containing and ubiquitylated plasma membrane proteins. Our results also imply that a Sla1 NPF motif adjacent to the SR region might regulate the Sla1–cargo interaction, mechanistically linking Sla1 cargo binding to endocytic site recruitment.

KEY WORDS: Endocytosis, Adaptor protein, Sorting signal, Ubiquitin, Yeast

INTRODUCTION

Clathrin-mediated endocytosis (CME) is a major mechanism by which eukaryotic cells internalize extracellular material and plasma membrane proteins (McMahon and Boucrot, 2011; Weinberg and Drubin, 2012). The selective and efficient uptake of integral membrane proteins depends on their interaction with components of the endocytic machinery termed adaptor proteins (Kirchhausen, 1999; Owen et al., 2004; Traub and Bonifacino, 2013). Besides binding and concentrating protein cargo at endocytic sites, adaptor proteins interact with other components of the endocytic machinery, such as clathrin, thereby constituting central players in the orchestration of CME (Reider and Wendland, 2011; Boettner et al., 2012; Lemmon and Traub, 2012). Sequential events of membrane invagination and scission result in internalization of a cargo-loaded clathrin-coated vesicle (Kukulski et al., 2012; Avinoam et al., 2015; Goode et al., 2015). Coat components, such as adaptors and clathrin, then dissociate from the vesicle, which is trafficked to endosomes, and the endocytic machinery is recruited back to the plasma membrane for repeated rounds of CME.

Many plasma membrane protein cargos contain short amino acid sequences that function as a sorting signal for recognition by the endocytic machinery. In *Saccharomyces cerevisiae*, two such peptide-based motifs have been established as capable of mediating cargo internalization. The NPFxD motif (where x indicates any amino acid) was the first endocytic signal characterized in yeast and is utilized for endocytosis of the cell wall stress sensor Wsc1 (also known as Slg1), the phospholipid flippases Drs2 and Dnf1, and the mating pheromone receptor Ste3 (Tan et al., 1996; Liu et al., 2007; Piao et al., 2007). It is likely that variations of this motif also work as endocytic signals. For example, the mating pheromone receptor Ste2 contains a functional NPFxD-related motif (GPFAD) (Howard et al., 2002). The NPFxD endocytic signal is recognized by the SHD1 domain of the clathrin adaptor protein Sla1 (Howard et al., 2002; Mahadev et al., 2007). More recently, the DxY motif was revealed as an endocytic signal present in the cell wall stress sensor Mid2, the peptide transporter Ptr2 and other cargos (Apel et al., 2017). The DxY endocytic signal is targeted by the μ-homology domain of the muniscin family adaptor protein Syp1 (Reider et al., 2009). Additionally, the Yxxϕ sequence (where ϕ indicates any bulky hydrophobic amino acid), which has been well characterized in mammalian cells and is recognized by AP-2, has been suggested to also function as an endocytic signal in yeast (Chapa-y-Lazo et al., 2014).

Although it has been demonstrated that peptide-based motifs designate integral membrane proteins for internalization by the endocytic machinery, it is not clear whether the signals play an active role in recruitment of the corresponding adaptor protein to the plasma membrane. In support of this possibility, *in vitro* experiments have shown that binding of mammalian AP-2 to synthetic liposomes is enhanced when the liposomes contain a lipid-linked endocytic signal peptide (Kelly et al., 2014). Additionally, it was shown in live mammalian cells that overexpression of an artificial cargo containing the NPxY endocytic signal enhances recruitment to the plasma membrane of the corresponding adaptors (ARH and DAB2), which were also overexpressed (Mettlen et al., 2010). Although these data suggest a role for endocytic signals in adaptor recruitment to the plasma membrane, a number of questions remain. For example, it would be important to test whether binding to endocytic signals contributes to adaptor recruitment *in vivo* in a native system in which proteins are expressed at endogenous levels.

A second means by which plasma membrane proteins are targeted for endocytosis is the covalent attachment of ubiquitin (Terrell et al., 1998). Plasma membrane proteins can be labelled to undergo CME by mono-ubiquitylation, multi-ubiquitylation (more than one lysine residue modified with an ubiquitin moiety) and poly-ubiquitylation with a chain of K63-linked ubiquitins. The yeast endocytic machinery components Ede1 and Ent1/Ent2 proteins contain well-established ubiquitin-binding domains, the ubiquitin-associated domain (UBA)

Department of Biochemistry and Molecular Biology, Colorado State University, Fort Collins, CO 80523-1870, USA.

*Author for correspondence (santiago.dipietro@colostate.edu)

S.M.D., 0000-0002-3372-8757

Handling Editor: Mahak Sharma
Received 17 April 2020; Accepted 27 August 2020

Journal of Cell Science (2020) 133, jcs247684. doi:10.1242/jcs.247684

and the ubiquitin-interacting motif (UIM), respectively (Reider and Wendland, 2011). Initial *in vitro* experiments suggested that Ede1 and Ent1 and Ent2 may be recruited to the plasma membrane and function as endocytic adaptors for ubiquitylated cargo proteins via their ubiquitin-binding domains (Aguilar et al., 2003). However, later *in vivo* experiments indicated these proteins may instead use their ubiquitin-binding domains to regulate themselves and the endocytic network (Aguilar et al., 2003; Dores et al., 2010). Ede1 was also shown to arrive at endocytic sites before cargo (Toshima et al., 2006). Thus, it is difficult to draw conclusions supporting the hypothesis of cargo binding dependence for Ede1 and Ent1/Ent2 recruitment to the plasma membrane. Furthermore, these experiments also implied that yeast endocytic machinery components other than or in addition to Ede1, Ent1 and Ent2 should be acting as adaptors for ubiquitylated cargo. Interestingly, the third SH3 domain of Sla1 (and that of its mammalian homolog CIN85, also known as SH3KBP1) is capable of binding ubiquitin *in vitro* (Stamenova et al., 2007). A functional role for the Sla1–ubiquitin interaction, however, remains to be explored.

A growing body of evidence from both yeast and mammalian systems supports the idea that cargo regulates progression between stages of endocytosis (Puthenveedu and von Zastrow, 2006; Layton et al., 2011; Carroll et al., 2012; Henry et al., 2012). Moreover, the existence of an endocytosis checkpoint has been proposed (Loerke et al., 2009; Aguet et al., 2013). Although the nature of this potential checkpoint is not well defined, it is believed to be responsive to cargo levels (Loerke et al., 2009; Mettlen et al., 2010). Thus, there is considerable interest in better understanding the interplay between cargo and the endocytic machinery. Sla1 is an attractive adaptor to study because, not only does it bind cargo and clathrin, it also regulates actin polymerization, thereby connecting key modules of the endocytic machinery (Holtzman et al., 1993; Rodal et al., 2003; Di Pietro et al., 2010; Feliciano and Di Pietro, 2012; Tolsma et al., 2018).

Here we explore the role of the endocytic signal NPFxD in the recruitment of its adaptor protein, Sla1. Point mutations of the NPFxD-binding surface of the Sla1 SHD1 domain that reduce the binding affinity to various degrees resulted in a proportional decrease of Sla1 recruitment to endocytic sites. Combination of the most severe SHD1 point mutations with deletion of the C-terminal region that links Sla1 to the endocytic machinery components Pan1 and End3 resulted in a complete loss of Sla1 recruitment to the plasma membrane. Interestingly, an NPF sequence in the Sla1 C-terminal region could bind the SHD1 domain intramolecularly, potentially acting as a regulatory mechanism for the Sla1–NPFxD interaction. The data further suggests that Sla1 may bind ubiquitylated cargo, and that ubiquitin binding could contribute to proper Sla1 recruitment to endocytic sites.

RESULTS

The SHD1 domain–NPFxD interaction contributes to Sla1 recruitment to the plasma membrane

Previous work demonstrated that Sla1 targets plasma membrane proteins for CME. Sla1 specifically binds the endocytic signal NPFxD through its SHD1 domain (Fig. 5A shows a diagram of Sla1 domains). This interaction mediates targeting of proteins that are completely or partially dependent upon Sla1 and the NPFxD signal for internalization such as Wsc1 and Ste3, respectively. NMR studies have demonstrated that the interaction between the SHD1 domain and NPFxD occurs through a predominantly hydrophobic pocket on the SHD1 surface (Mahadev et al., 2007). Moreover, the relative contribution of individual SHD1 binding pocket residues to the interaction has been determined by analyzing point mutants in NPFxD binding assays *in vitro* and various functional assays *in vivo* (Mahadev et al., 2007). For example, mutation of Sla1 amino acid K525 reduces affinity for the NPFxD sequence from 6 µM to 195 µM, whereas mutation of residue F507 or I531 abolishes binding (Mahadev et al., 2007). This work presented us with an ideal system to determine whether cargo binding contributes to Sla1 recruitment to the plasma membrane. We reasoned that Sla1–GFP carrying mutations of the same SHD1 residues would allow testing for a Sla1 recruitment defect while maintaining all other Sla1 domains and interactions intact. Accordingly, strains expressing Sla1–GFP and point mutants Sla1^{K525A}–GFP, Sla1^{F507L}–GFP, or Sla1^{I531E}–GFP from the *SLA1* endogenous locus were generated. Immunoblotting analysis of total cell extracts indicated that the stability and overall expression level of various mutants was comparable to wild-type Sla1–GFP (Fig. S1). The plasma membrane recruitment of wild-type Sla1–GFP and each of the mutants was analyzed by live-cell confocal fluorescence microscopy (Fig. 1). The maximal Sla1–GFP fluorescence intensity achieved at endocytic sites, as well as the overall Sla1–GFP fluorescence intensity measured across the entire plasma membrane, was quantified (Fig. 1). Whereas no defect was observed with Sla1^{K525A}–GFP, the levels of Sla1^{F507L}–GFP and Sla1^{I531E}–GFP were reduced. Thus, the SHD1 mutations that most severely affect NPFxD binding cause a reduction in Sla1 recruitment to the plasma membrane (Fig. 1). Consistently, quantification of the total number of endocytic patches per cell showed no defect for Sla1^{K525A}–GFP (mean±s.e.m.; 10.5±0.4 patches, n=35 cells, P=0.20) but a reduction for Sla1^{F507L}–GFP (9.7±0.4 patches, n=43 cells, P=0.009) and Sla1^{I531E}–GFP (9.0±0.3 patches, n=44 cells, P=0.0005) relative to Sla1–GFP (11.3±0.4 patches, n=42 cells).

Sla1 was previously reported to undergo nucleocytoplasmic shuttling (Gardiner et al., 2007). During the course of these experiments, we observed Sla1 localizing to an internal structure reminiscent of the nucleus. This was more evident for Sla1^{I531E}–GFP and to a lesser extent Sla1^{F507L}–GFP, the two mutants that most severely affected recruitment to endocytic sites (Fig. 1). Nuclear localization was confirmed using two-color fluorescence microscopy imaging of Nup133–mCherry, a component of the nuclear pore complex, and Sla1–GFP wild type and corresponding SHD1 mutants (Fig. S2). Quantification demonstrated that the level of nuclear localization for each Sla1–GFP mutant correlated with the degree to which membrane recruitment was reduced (Fig. S2).

The SHD1 domain–NPFxD interaction and SR region are essential for Sla1 recruitment to the plasma membrane

The Sla1 C-terminal LxxQxTG repeat region (SR) mediates interactions with key coat proteins Pan1 and End3 contributing to the recruitment of Sla1 to endocytic sites (Tang et al., 2000; Chi et al., 2012; Sun et al., 2015). Accordingly, a truncated form of Sla1 missing the SR region (Sla1ΔSR–GFP) has previously been shown to localize to the plasma membrane but in a more diffuse fashion, not efficiently concentrated at endocytic sites. We generated cells expressing Sla1ΔSR–GFP from the endogenous *SLA1* locus and reproduced those results here (Fig. 2). Interestingly, the overall levels of Sla1ΔSR–GFP quantified across the entire plasma membrane are higher than wild-type Sla1–GFP, rather than lower (Fig. 2). Based on the results presented in Fig. 1, we hypothesized that Sla1ΔSR–GFP is recruited from the cytosol to the plasma membrane in a broad manner via interaction with NPFxD-containing membrane proteins. To test this idea, we followed two approaches.

First, we performed fluorescence recovery after photobleaching (FRAP) experiments with cells expressing either Sla1ΔSR–GFP or the integral membrane protein Ste2–GFP from the corresponding endogenous locus. After photobleaching a portion of the plasma

Journal of Cell Science (2020) 133, jcs247684. doi:10.1242/jcs.247684

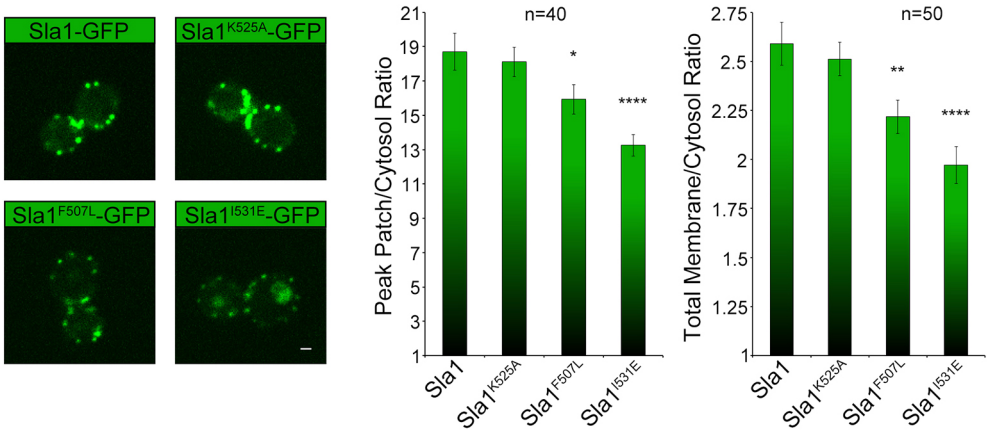

Fig. 1. The SHD1 domain–NPFxD interaction contributes to Sla1 recruitment to the plasma membrane. Live-cell confocal fluorescence microscopy analysis of yeast cells expressing either Sla1–GFP (SDY1422), Sla1^{K525A}–GFP (SDY603), Sla1^{F507L}–GFP (SDY601) or Sla1^{I531E}–GFP (SDY599) from the endogenous *SLA1* locus. Left, panels show representative frames from each strain. Middle, quantification represented as peak patch to cytosol ratio of fluorescence intensity at endocytic sites was performed as described in the Materials and Methods. A decreased recruitment is observed with the two SHD1 mutants that more severely disrupt binding to NPFxD, Sla1^{F507L}–GFP and Sla1^{I531E}–GFP (n=40 patches; P=0.6624 for Sla1^{K525A}–GFP, P=0.0477 for Sla1^{F507L}–GFP, P<0.0001 for Sla1^{I531E}–GFP). Right, quantification represented as total membrane to cytosol ratio of fluorescence intensity across the entire cell plasma membrane was performed as described in the Materials and Methods. The quantification demonstrates a recruitment defect for Sla1^{F507L}–GFP and Sla1^{I531E}–GFP (n=50 cells; P=0.1713 for Sla1^{K525A}–GFP, P<0.0001 for Sla1^{F507L}–GFP, P<0.0001 for Sla1^{I531E}–GFP). The internal structure most visible with Sla1^{I531E}–GFP corresponds to the nucleus (see Fig. S2). Scale bar: 1 µm. Data are mean±s.e.m. *P<0.05, **P<0.01, ****P<0.0001 (unpaired Student's t-test).

membrane, Sla1ΔSR–GFP recovered quickly but Ste2–GFP did not (Fig. 3A). FRAP experiments with cells expressing both Sla1ΔSR–GFP and the coat protein Pan1–RFP showed that Sla1ΔSR–GFP was present and then recovered at locations across the membrane, both showing Pan1–RFP (endocytic sites) and not showing Pan1–RFP (outside endocytic sites) (Fig. 3B). The data suggest that Sla1ΔSR–GFP is recruited broadly from the cytosol to the plasma membrane and that the soluble and membrane-bound pools of Sla1ΔSR–GFP exchange quickly. On the other hand, the Ste2–GFP FRAP result indicates that lateral diffusion of Sla1ΔSR–GFP while bound to integral membrane proteins is likely limited. Interestingly, although Sla1ΔSR–GFP is more diffusely localized across the plasma membrane than wild-type Sla1–GFP, it does show a patchy localization. It is possible that Sla1ΔSR–GFP is preferentially

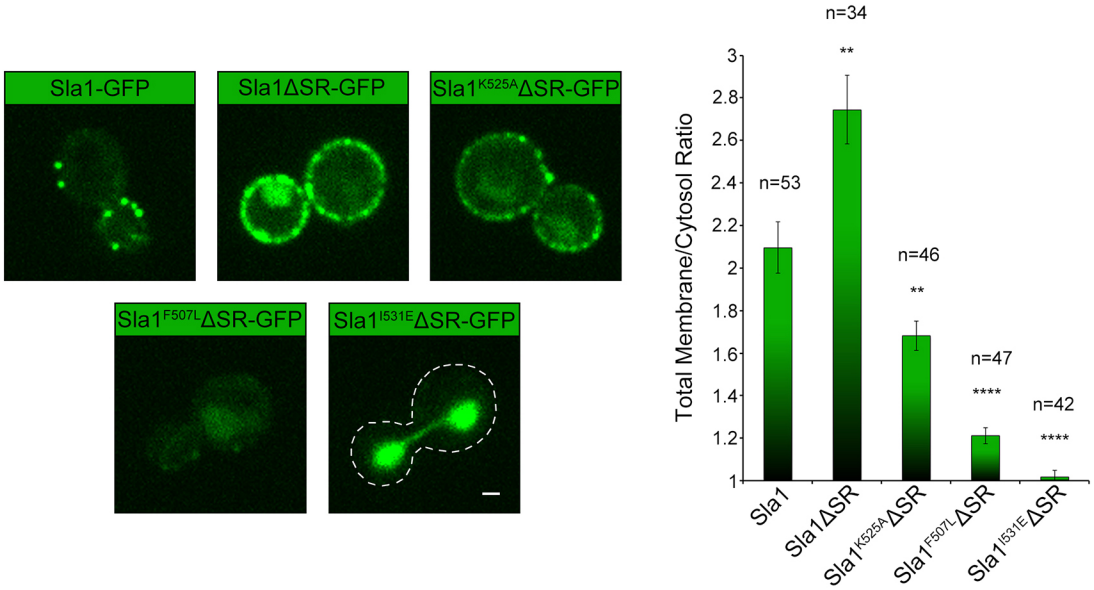

Fig. 2. The SHD1–NPFxD and SR–Pan1/End3 interactions are required for Sla1 recruitment to the plasma membrane. Live-cell confocal fluorescence microscopy analysis of cells expressing either Sla1–GFP (GPY4914), Sla1ΔSR–GFP (SDY712), Sla1^{K525A}ΔSR–GFP (SDY738), Sla1^{F507L}ΔSR–GFP (SDY736) or Sla1^{I531E}ΔSR–GFP (SDY718) from the endogenous *SLA1* locus. Left, panels show representative frames from each strain. Right, quantification represented as total membrane to cytosol ratio of fluorescence intensity across the entire cell plasma membrane, showing that deletion of the SR region alone results in broad and higher levels of membrane localization. However, SR deletion in combination with mutation of the NPFxD-cargo binding surface of SHD1 reduces Sla1 recruitment to the plasma membrane more than the same SHD1 mutations alone (n=53 cells for Sla1; n=34 cells for Sla1ΔSR–GFP, P=0.0015; n=46 cells for Sla1^{K525A}ΔSR–GFP, P=0.0054; n=47 cells for Sla1^{F507L}ΔSR–GFP, P<0.0001; n=42 cells for Sla1^{I531E}ΔSR–GFP, P<0.0001). Note that the most severe mutants, Sla1^{F507L}ΔSR–GFP and Sla1^{I531E}ΔSR–GFP, are largely absent from the plasma membrane. Scale bar: 1 µm. Data are mean±s.e.m. **P<0.01, ****P<0.0001 (unpaired Student's t-test).

Journal of Cell Science (2020) 133, jcs247684. doi:10.1242/jcs.247684

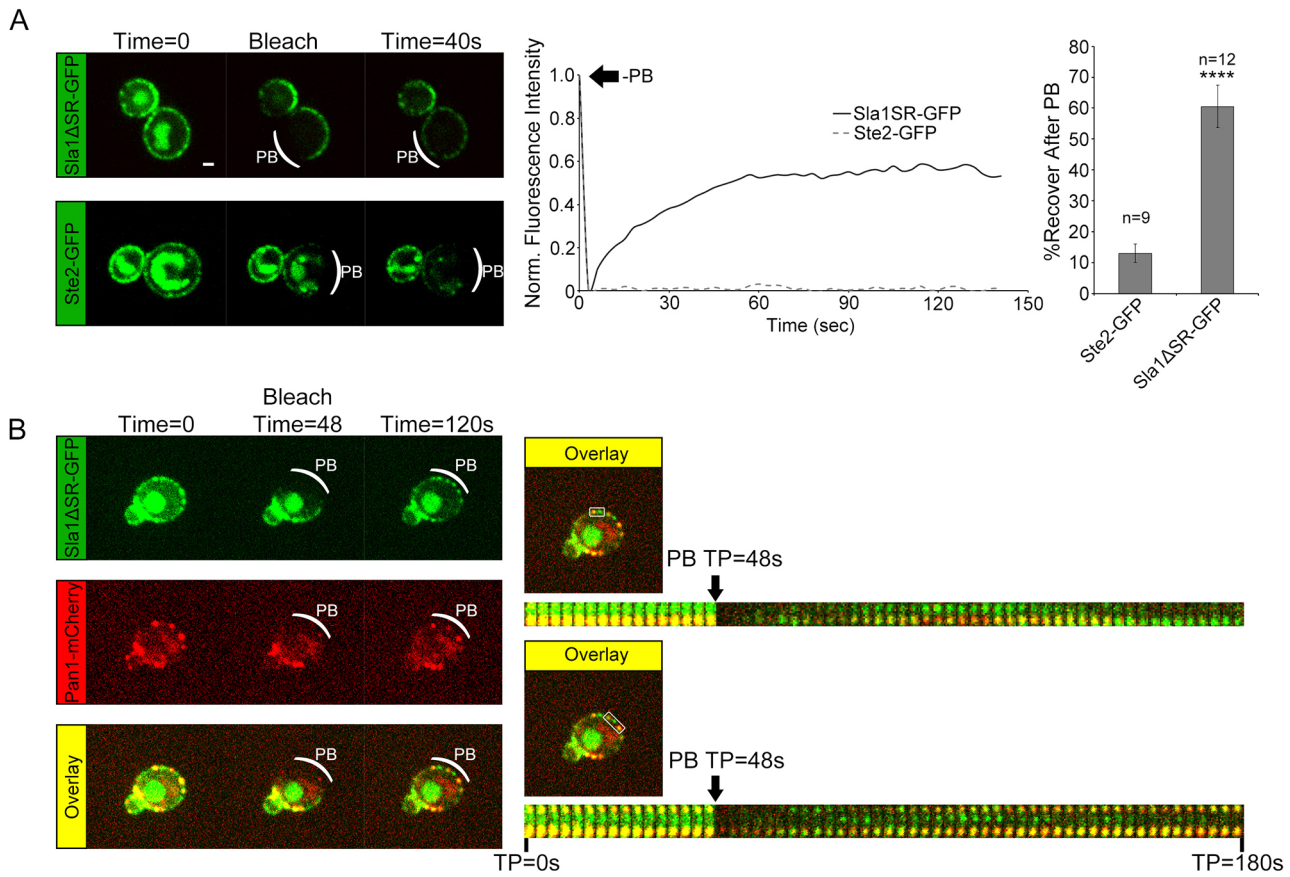

Fig. 3. Sla1ΔSR–GFP is recruited broadly from the cytosol to the plasma membrane. (A) Fluorescence recovery after photobleaching (FRAP) experiments with cells expressing either Sla1ΔSR–GFP (SDY712) or Ste2–GFP (SDY783) from the corresponding endogenous locus. Left, representative frames of Sla1ΔSR–GFP and Ste2–GFP before (time=0), immediately after (bleach) and 40 s post photobleaching (PB). The area indicated by a curved white line was subjected to photobleaching. Center, graphical representation of Sla1ΔSR–GFP and Ste2–GFP FRAP. Right, quantification, represented as bar graphs, of the maximal FRAP value obtained after 150 s post photobleaching (n=12 cells for Sla1ΔSR–GFP and n=9 cells for Ste2–GFP, P<0.0001). Bar graph shows mean±s.e.m. ****P<0.0001 (unpaired Student's t-test). (B) FRAP imaging of cells expressing both Sla1ΔSR–GFP and Pan1–RFP (SDY913) from their corresponding endogenous loci. Left, representative frames of Sla1ΔSR–GFP and Pan1–RFP before (Time=0), immediately after (Bleach Time=48), and 72 s after photobleaching. The area indicated by a curved white line was subjected to photobleaching. Right, kymographs of Sla1ΔSR–GFP and Pan1–RFP photobleaching and recovery from cells represented on the left. Regions of cells used to make the kymographs are labeled with white rectangles. TP, time point. Scale bar for A and B: 1 µm.

recruited to plasma membrane regions where cargo is more concentrated.

Second, we generated cells that combined the SR deletion with SHD1 binding pocket point mutations described above (K525A, F507L and I531E) in the *SLA1* endogenous gene. Immunoblotting analysis of total cell extracts indicated that the stability and overall expression level of the mutants was comparable to wild-type Sla1-GFP (Fig. S1). Visual inspection of live-cell fluorescence microscopy images suggested each of the SHD1 mutations had a more dramatic effect on Sla1–GFP recruitment to the plasma membrane when combined with the SR deletion than alone (Figs 1, 2). This observation was confirmed by quantification of the Sla1–GFP fluorescence across the plasma membrane (Figs 1, 2). Furthermore, the most severe mutants ($Sla1^{F507L}$ΔSR–GFP and $Sla1^{I531E}$ΔSR–GFP) showed negligible plasma membrane recruitment (Fig. 2).

From these experiments, we conclude that the SR–Pan1–End3 interaction works cooperatively with the SHD1–NPFxD cargo interaction to recruit Sla1. The results suggest that SHD1–NPFxD cargo binding contributes to general and broad recruitment of Sla1 to the plasma membrane, while interactions with Pan1/End3 specify recruitment of Sla1 to endocytic sites.

Multiple interactions with cargo and/or other endocytic machinery proteins are needed for Sla1 recruitment to the plasma membrane

To test whether the Sla1 SHD1 domain by itself is capable of plasma membrane recruitment, we expressed SHD1–GFP from a plasmid in wild-type cells. Live-cell fluorescence microscopy imaging showed no detectable recruitment of the SHD1 domain to the plasma membrane (Fig. 4A). However, similar constructs expressing two or three SHD1 domain copies in tandem (2×SHD1–GFP and 3×SHD1–GFP) did localize to the plasma membrane, preferentially to the bud, suggesting multiple interactions are needed for effective recruitment (Fig. 4A).

In *sla1Δ* cells, NPFxD–Sla1-dependent cargo such as Wsc1–GFP accumulates at the plasma membrane (Piao et al., 2007). At least for Wsc1–GFP, this is also accompanied by loss of polarized localization (Mahadev et al., 2007; Piao et al., 2007). Expression of 2×SHD1–GFP and 3×SHD1–GFP in *sla1Δ* cells demonstrated a higher overall level of recruitment across the plasma membrane compared to that in wild-type cells (Fig. 4A). The data supports the idea that these artificial constructs are indeed binding to plasma membrane proteins containing the NPFxD signal and that multiple interactions are needed for recruitment.

Journal of Cell Science (2020) 133, jcs247684. doi:10.1242/jcs.247684

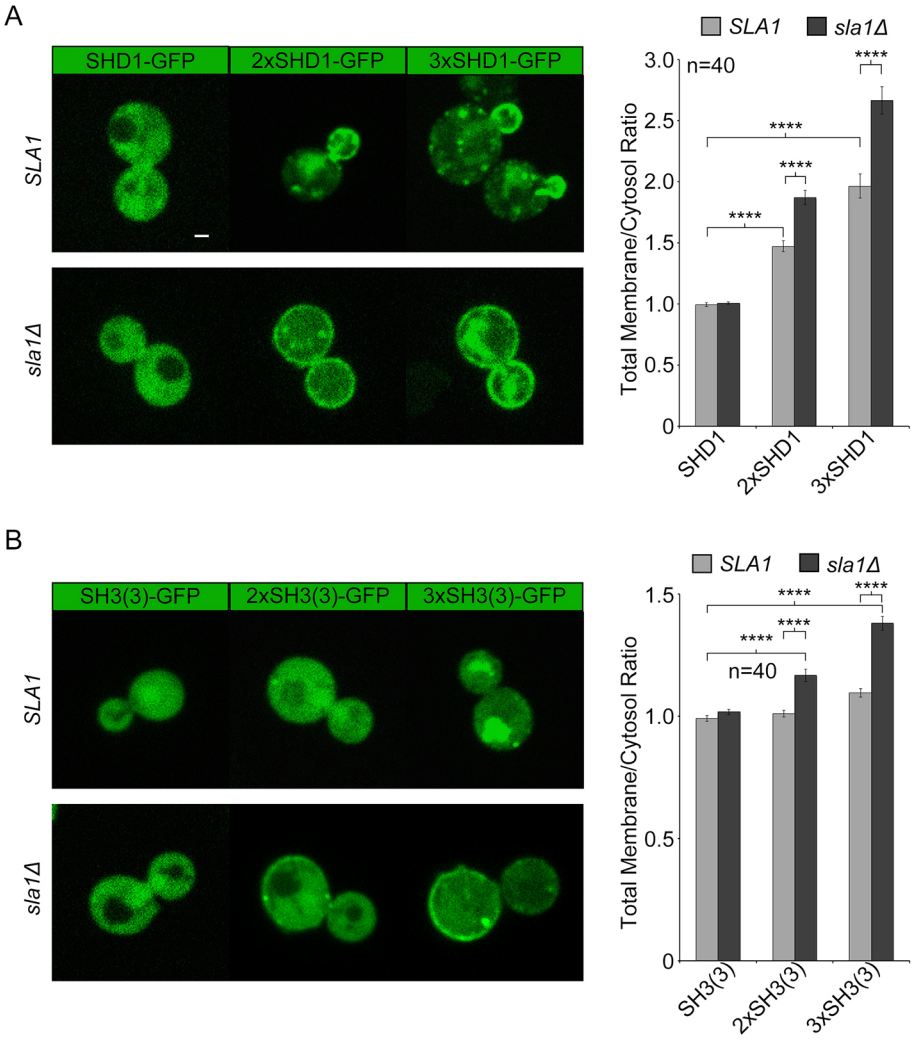

Fig. 4. Multiple copies in tandem of the Sla1 SHD1 domain or the Sla1 SH3(3) domain are capable of plasma membrane recruitment. (A) Left, images of SHD1–GFP, 2×SHD1–GFP or 3×SHD1–GFP expressed from high copy plasmids (pSDP904, pSDP1059 and pSDP1061, respectively) in either wild-type (*SLA1*) or *sla1Δ* cells. Right, quantification of the total membrane to cytosol ratio of fluorescence intensity across the entire cell plasma membrane. 2×SHD1–GFP and 3×SHD1–GFP are capable of plasma membrane recruitment, as demonstrated by the increased total membrane to cytosol ratio in both wild-type and *sla1Δ* cells (n=40 cells, P<0.0001 for 2×SHD1–GFP and 3×SHD1–GFP in wild-type and *sla1Δ* cells). The total membrane to cytosol ratio increased for 2×SHD1–GFP and 3×SHD1–GFP in *sla1Δ* cells when compared to that in wild-type cells (*SLA1*) (n=40, P<0.0001). (B) Left, images of SH3(3)–GFP, 2×SH3(3)–GFP or 3×SH3(3)–GFP expressed from high copy plasmids (pSDP978, pSDP1060 and pSDP1062, respectively) in either wild-type (*SLA1*) or *sla1Δ* cells. Right, quantification of the total membrane to cytosol ratio of fluorescence intensity across the entire cell plasma membrane. 2×SH3(3)–GFP and 3×SH3(3)–GFP are capable of plasma membrane recruitment only in *sla1Δ* cells, as demonstrated by an increase in the total membrane to cytosol ratio (n=40, P<0.0001 for 2×SH3(3)–GFP and 3×SH3(3)–GFP). Scale bar for A and B: 1 µm. Data are mean±s.e.m. ****P<0.0001 (unpaired Student's t-test).

Although these experiments suggest more than one Sla1–cargo protein interaction may be needed for efficient recruitment to the plasma membrane, Sla1 only has one SHD1 domain. Yet, Sla1ΔSR–GFP is broadly recruited to the plasma membrane in a cargo binding-dependent manner. We therefore considered the possibility that the third Sla1 SH3 domain, which binds ubiquitin *in vitro*, may bind ubiquitylated plasma membrane proteins and potentially contribute to membrane recruitment.

To test whether the third Sla1 SH3 domain [SH3(3)] by itself is capable of plasma membrane recruitment, we expressed SH3(3)–GFP from a plasmid in wild-type cells. Live-cell fluorescence microscopy imaging demonstrated no detectable recruitment of SH3(3)–GFP to the plasma membrane (Fig. 4B). Similarly, constructs expressing two or three SH3(3) domain copies in tandem [2×SH3(3)–GFP and 3×SH3(3)–GFP, respectively] in wild-type cells also resulted in cytosolic localization (Fig. 4B). However, expression of 2×SH3(3)–GFP and 3×SH3(3)–GFP in *sla1Δ* cells, which accumulate endocytic cargo on the cell surface, did demonstrate broad plasma membrane localization (Fig. 4B). This result suggests SH3(3) might be able to bind ubiquitylated plasma membrane proteins, and perhaps cooperate with SHD1 in recruiting Sla1 to the plasma membrane.

Indeed, Sla1 fragments containing SH3(3) and SHD1 efficiently and broadly localized to the plasma membrane in wild-type cells (Fig. 5A,B; Frag 1–GFP, Frag 2–GFP and Frag 3–GFP). Frag 3–GFP is particularly informative because it only includes the SH3(3) and SHD1 domains, suggesting that the ability to simultaneously bind ubiquitylated and NPFxD-containing membrane proteins is sufficient for plasma membrane recruitment. Parallel experiments with SH3(3) alone (Frag 4–GFP) and SHD1 alone (Frag 5–GFP) confirmed that each domain by itself is not efficiently recruited to the plasma membrane (Fig. 5A,B).

To further test the idea that Frag 3–GFP is recruited to the plasma membrane via interaction with ubiquitylated and NPFxD-containing proteins, point mutations known to hinder ubiquitin or NPFxD binding were introduced in the Frag 3–GFP expression plasmid. Mutation W391A in the SH3(3) domain, which has been shown to reduce ubiquitin binding *in vitro* (Stamenova et al., 2007), significantly diminished recruitment of Frag 3–GFP to the plasma membrane (Fig. 5B, Frag 3^{W391A}–GFP). Recruitment was completely eliminated when mutation I531E of the SHD1 was introduced into Frag 3–GFP (Fig. 5C, Frag 3^{I531E}-GFP), indicating that the SHD1 domain plays a more significant role in recruitment to the plasma membrane.

We then introduced the W391A mutation in the context of full-length Sla1–GFP at the endogenous locus in otherwise wild-type cells. This mutation did not affect protein stability or expression level (Fig. S1). The plasma membrane recruitment of $Sla1^{W391A}$–GFP was compared with that of wild-type Sla1–GFP and $Sla1^{I531E}$–GFP, also expressed from the endogenous *SLA1* locus. Live-cell fluorescence microscopy analysis and quantification showed a modest but

Journal of Cell Science (2020) 133, jcs247684. doi:10.1242/jcs.247684

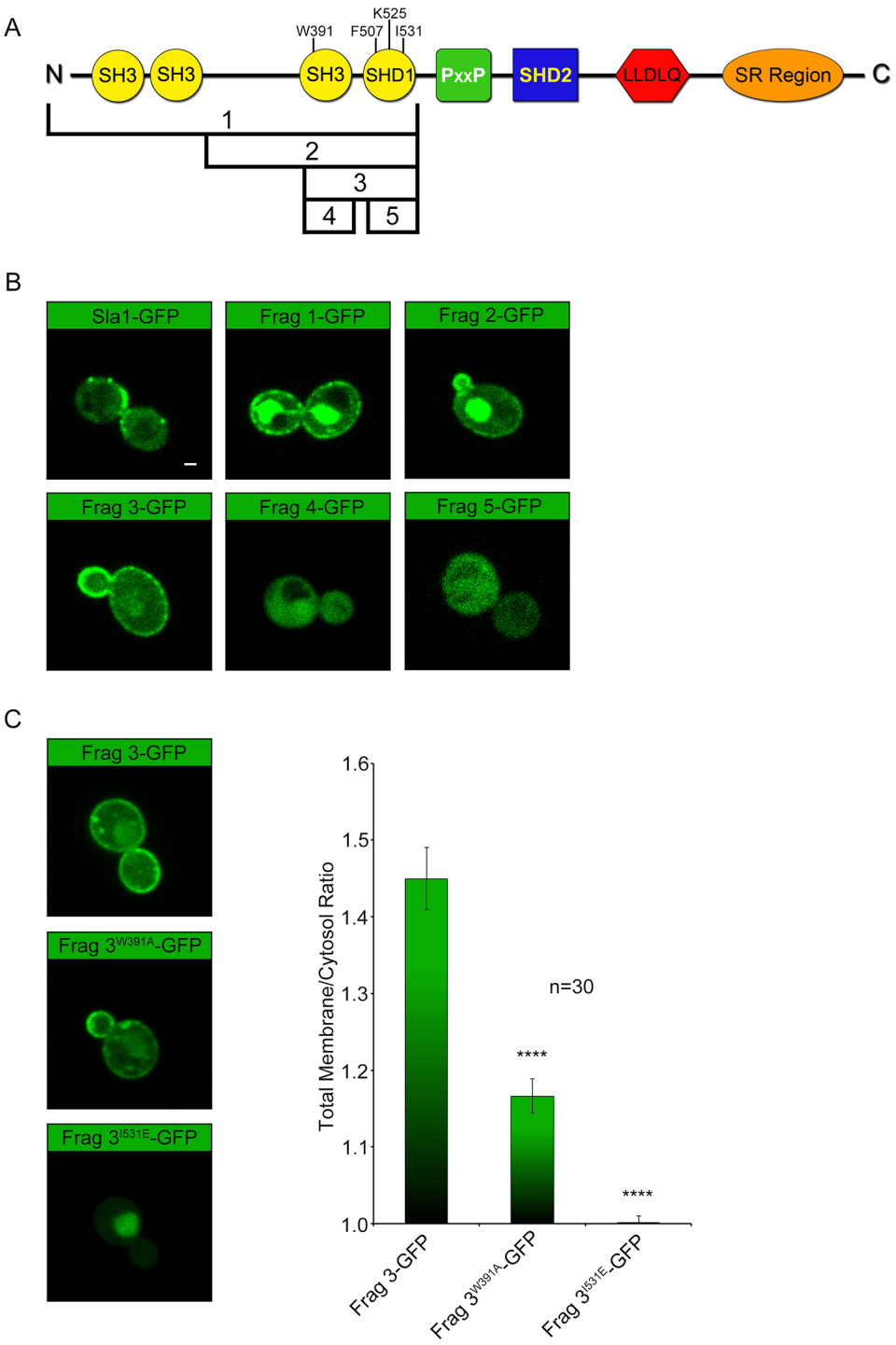

Fig. 5. The minimal fragment of Sla1 containing both the SH3(3) and SHD1 domains is capable of plasma membrane recruitment. (A) Diagram of Sla1 domains. SH3(3) and SHD1 amino acids subjected to mutagenesis are labeled. Numbered brackets indicate fragments of Sla1 analyzed in the experiments shown in Fig. 5B. (B) Live-cell confocal fluorescence microscopy analysis of wild-type yeast cells expressing fragments of Sla1 fused to GFP. Sla1 full length and Sla1 fragments were exogenously expressed with a GFP tag from high copy plasmids: Sla1–GFP (pSDP965), Frag 1–GFP (pSDP964), Frag 2–GFP (pSDP963), Frag 3–GFP (pSDP962), Frag 4–GFP (pSDP978) and Frag 5–GFP (pSDP904). All fragments containing both the SH3(3) and SHD1 domains were shown to localize to the plasma membrane. (C) Left, live-cell confocal fluorescence microscopy analysis of Frag 3–GFP (pSDP962), Frag 3–GFP containing an SH3(3) mutation shown to reduce ubiquitin binding by SH3(3) (Frag 3^{W391A}–GFP, pSDP979), and Frag 3–GFP containing the I531E mutation shown to reduce NPFxD binding by SHD1 (Frag 3^{I531E}–GFP, pSDP1054). Right, quantification of total membrane to cytosol ratio of fluorescence intensity across the entire cell plasma membrane for Frag 3–GFP and the corresponding mutants (n=30 cells; P<0.0001 for Frag 3^{W391A}–GFP, P<0.0001 for Frag 3^{I531E}–GFP). Scale bar for B and C: 1 µm. Data are mean±s.e.m. ****P<0.0001 (unpaired Student's t-test).

statistically significant recruitment defect for $Sla1^{W391A}$–GFP relative to recruitment of the wild type (Fig. 6). Paralleling the data obtained with Frag 3–GFP (Fig. 5), the recruitment defect demonstrated by $Sla1^{W391A}$–GFP was less pronounced than that of $Sla1^{I531E}$–GFP (Fig. 6).

Overall, the data suggest that both SH3–ubiquitin and SHD1–NPFxD interactions contribute to Sla1 recruitment to the plasma membrane, with the latter having a more significant role. This difference in relative importance is consistent with the fact that the SH3(3)–ubiquitin interaction (40 µM) is weaker than the SHD1–NPFxD interaction (6 µM) (Mahadev et al., 2007; Stamenova et al., 2007).

Potential negative regulation by a Sla1 C-terminal NPF motif

Based on the above results, it is puzzling that full-length Sla1 does not broadly coat the plasma membrane in the same way that Sla1ΔSR–GFP or Frag 3–GFP do. The data suggest that the Sla1 SR region contributes to cytosolic Sla1 remaining in a state that is not recruited directly to the plasma membrane through interactions with cargo. One possibility is that properties of the Sla1 C-terminal region that are lost in Sla1ΔSR–GFP negatively regulate interactions with ubiquitylated and/or NPFxD-containing membrane proteins.

Interestingly, we observed that Sla1 contains a C-terminal NPFGF-COOH sequence, which follows the LxxQxTG repeats and is deleted in Sla1ΔSR–GFP. We hypothesized that the NPFGF-

Journal of Cell Science (2020) 133, jcs247684. doi:10.1242/jcs.247684

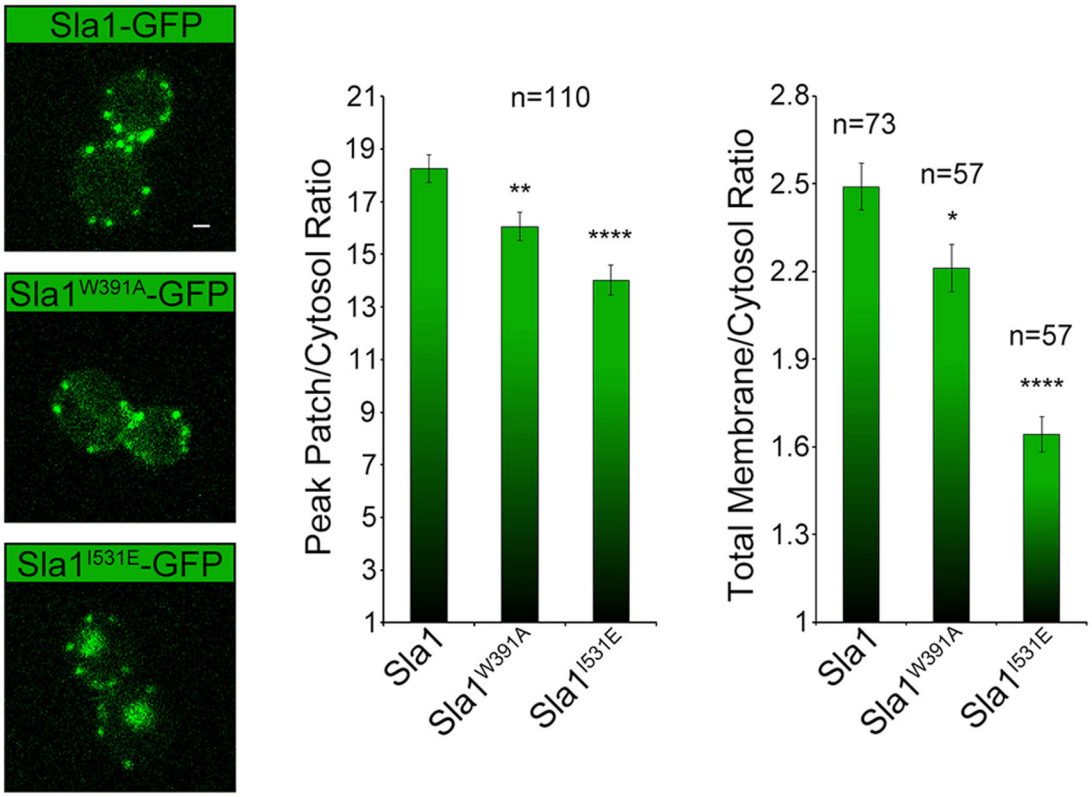

Fig. 6. Binding to ubiquitylated proteins contributes to optimal Sla1 recruitment to the plasma membrane. Live-cell confocal fluorescence microscopy analysis of yeast cells expressing either Sla1–GFP (GPY4914), Sla1^{W391A}–GFP (SDY832) or Sla1^{I531E}–GFP (SDY542) from the endogenous *SLA1* locus. Left, panels show representative frames from each strain. Middle, quantification represented as peak patch to cytosol ratio of fluorescence intensity at endocytic sites (n=110 patches; P=0.0036 for Sla1^{W391A}–GFP, P<0.0001 for Sla1^{I531E}–GFP). Right, quantification represented as total membrane to cytosol ratio of fluorescence intensity across the entire cell plasma membrane (n=73 cells for Sla1–GFP, n=57 cells for Sla1^{W391A}–GFP and n=57 cells for Sla1^{I531E}–GFP; P=0.0036 for Sla1^{W391A}–GFP, P<0.0001 for Sla1^{I531E}–GFP). A decreased recruitment is observed with the SH3(3) mutant that disrupts ubiquitin binding, but this defect is less pronounced than the one observed for the SHD1 mutant unable to bind NPFxD. Scale bar: 1 µm. Data are mean±s.e.m. *P<0.05, **P<0.01, ****P<0.0001 (unpaired Student's t-test).

COOH sequence might assist in regulating cargo binding and Sla1-membrane recruitment by competing for SHD1 binding. To test this possibility, we performed three experiments.

First, we previously established a GST-pulldown assay to test for SHD1 binding to the NPFxD signal. Purified recombinant SHD1 binds to GST fused to a triple repeat of the endocytic signal active form (GST–3×NPFSD) but does not bind to the corresponding inactive form (GST–3×NPASD) (Mahadev et al., 2007). We reproduced this result here and found that, as expected, SHD1 containing the I531E mutation does not bind to GST–3×NPFSD (Fig. 7A,B; SHD1^{I531E}). To test for a possible autoinhibition, a construct was generated in which the last 31 amino acids of Sla1, containing the NPFGF-COOH sequence, were fused to the SHD1 domain (SHD1–NPFGF*). We also generated the corresponding F-to-A point mutant (SHD1–NPAGF*) that should not bind SHD1. GST pulldown assays showed that although both SHD1–NPFGF* and SHD1–NPAGF* were able to bind to GST–3×NPFSD, the interaction was much weaker for SHD1–NPFGF* (Fig. 7A,B).

Second, the last 31 amino acids of Sla1, containing the NPFGF-COOH sequence, were introduced into Frag 3–GFP to generate the Frag 3–NPFGF–GFP expression plasmid. Expression of Frag 3–NPFGF–GFP in wild-type cells, live-cell imaging and quantification of membrane recruitment demonstrated a significant reduction in recruitment compared with that of Frag 3–GFP fragment (Fig. 7C).

Third, if the Sla1 C-terminal NPFGF-COOH sequence inhibits interaction between SHD1 and NPFxD-containing plasma membrane proteins, mutation of the NPFGF-COOH sequence might rescue Sla1-SHD1 mutants displaying a partial recruitment defect, such as Sla1^{F507L}–GFP (Fig. 1). To test this possibility, we generated cells that combined a deletion of the NPFGF-COOH sequence with the SHD1 point mutation F507 L in the *SLA1* endogenous gene (Sla1^{F507L}ΔNPFGF–GFP). We also generated cells harboring only a deletion of the NPFGF-COOH sequence (Sla1ΔNPFGF–GFP). Immunoblotting analysis of total cell extracts indicated that the stability and overall expression level of these mutants was comparable to wild-type Sla1–GFP (Fig. S1). Fluorescence microscopy analysis showed that the plasma membrane levels of Sla1^{F507L}ΔNPFGF–GFP were higher than those of Sla1^{F507L}–GFP – although lower than those of wild-type Sla1–GFP – suggesting that mutation of the NPFGF-COOH sequence indeed elicited a partial rescue (Fig. S3). Mutation of the NPFGF-COOH sequence alone (Sla1ΔNPFGF–GFP) caused a modest but statistically significant decrease in plasma membrane recruitment relative to recruitment of Sla1–GFP (Fig. S3).

Taken together, the data suggest that a C-terminally located NPFGF motif has the potential to bind intramolecularly to SHD1 and negatively regulate interaction with plasma membrane proteins harboring the NPFxD endocytic signal.

Disruption of the Sla1–NPFxD interaction affects progression of endocytosis

We wanted to assess whether the lower levels of Sla1 recruitment to the plasma membrane caused by its inability to bind cargo affected

Journal of Cell Science (2020) 133, jcs247684. doi:10.1242/jcs.247684

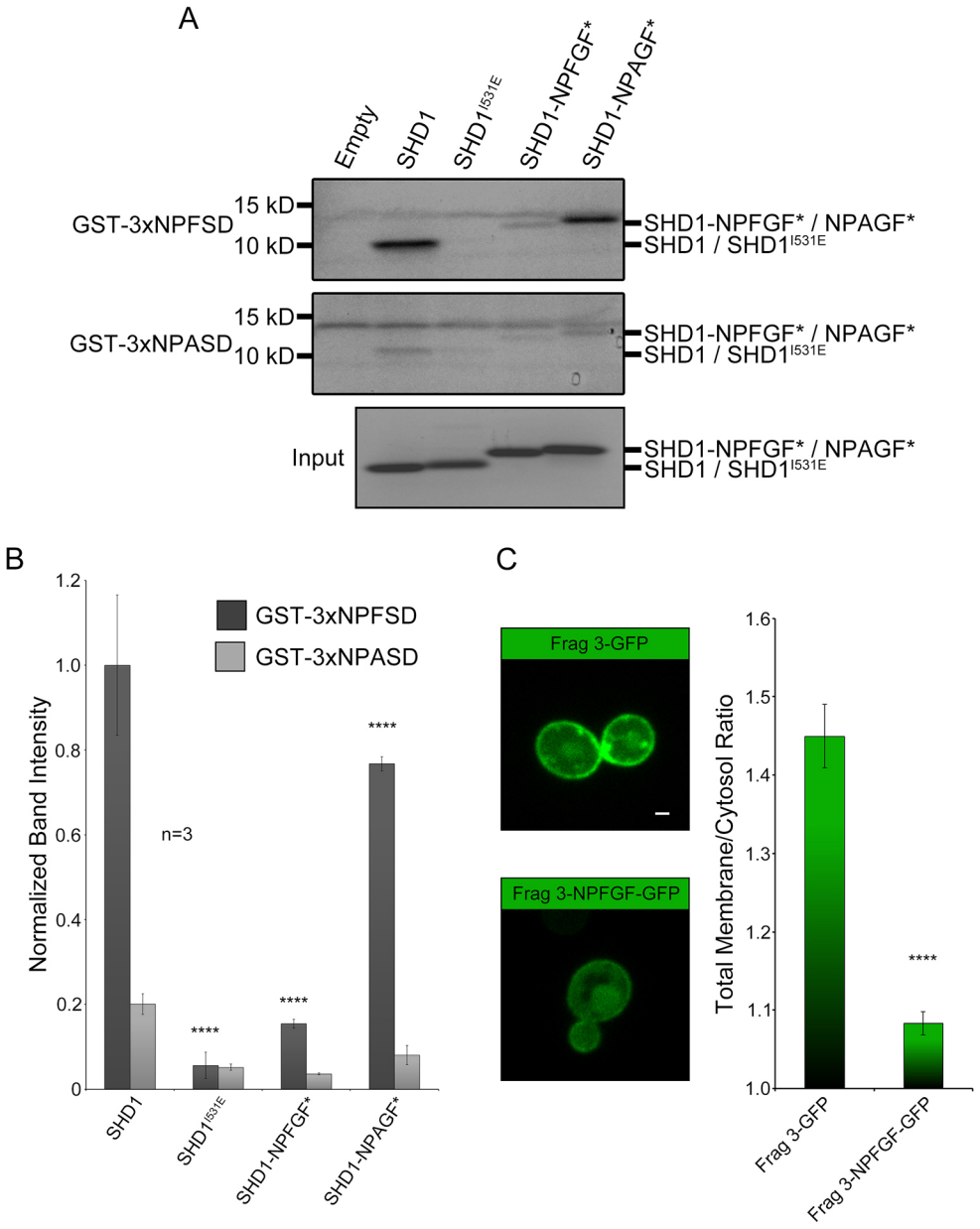

Fig. 7. The NPFGF-COOH sequence at the Sla1 C-terminus is capable of competing with the NPFxD endocytic signal for binding to SHD1. GST–3×NPFSD and GST–3×NPASD were bound to glutathione beads, and pulldown experiments were performed using polyhistidine-tagged SHD1; SHD1^{I531E}, a fusion protein in which the last 31 amino acids of Sla1, containing the NPFGF-COOH sequence, were attached to the SHD1 domain (SHD1–NPFGF*); or the corresponding SHD1–NPAGF* fusion mutant. (A) Top, the SHD1 domain binds to the active form of the endocytic signal (GST–3×NPFSD) but not the inactive mutant form (GST–3×NPASD). Mutation of residue I531E in the SHD1 domain eliminated binding. The SHD1–NPFGF* fusion was able to bind GST–3×NPFSD, but more weakly than SHD1–NPAGF* suggesting self-inhibition by the NPFGF-COOH sequence. Middle, all SHD1 fragments, mutants and fusions showed little to no binding to GST–3×NPASD. Bottom, input loading controls for polyhistidine-tagged proteins SHD1, SHD1^{I531E}, SHD1–NPFGF* and SHD1–NPAGF*. (B) Quantification of normalized band intensities of each polyhistidine-tagged protein binding to either GST–3×NPFSD or GST–3×NPASD mutant (n=3; P<0.0001 for fragments SHD1, SHD1^{I531E}, SHD1–NPFGF* and SHD1–NPAGF* binding to GST–3×NPFSD). (C) Left, live-cell confocal fluorescence microscopy analysis of wild-type yeast cells expressing Frag 3–GFP or a modified version of Frag 3–GFP in which the last 31 residues of Sla1 containing the NPFGF-COOH C-terminal sequence were inserted between Frag 3 and GFP (Frag 3–NPFGF–GFP, pSDP997). Right, quantification of total membrane to cytosol ratio of fluorescence intensity across the entire cell plasma membrane for Frag 3–GFP and Frag 3–NPFGF–GFP (P<0.0001, 30 cells per strain). Scale bar: 1 µm. Data are mean±s.e.m. ****P<0.0001 (unpaired Student's t-test).

other components of the endocytic machinery. Thus, we generated a strain expressing Sla1^{I531E}–mCherry and Pan1–GFP from the corresponding endogenous loci and performed live-cell fluorescence microscopy analysis. The patch lifetime of Pan1–GFP (mean±s.e.m., 53.2±2.0 s, P<0.0001) was prolonged compared with that in wild-type cells (41.7±1.3 s), indicating a mild but noticeable defect in endocytic progression (Fig. 8).

DISCUSSION

A long-held view of endocytosis poses that the endocytic machinery assembles on the cytosolic leaflet of the plasma membrane, and then cargo is bound and internalized. Emerging evidence, however, suggests that cargo is not a passive player but may in fact help recruit endocytic adaptors and regulate the overall process (Loerke et al., 2009; Mettlen et al., 2010; Layton et al., 2011; Carroll et al., 2012;

Journal of Cell Science (2020) 133, jcs247684. doi:10.1242/jcs.247684

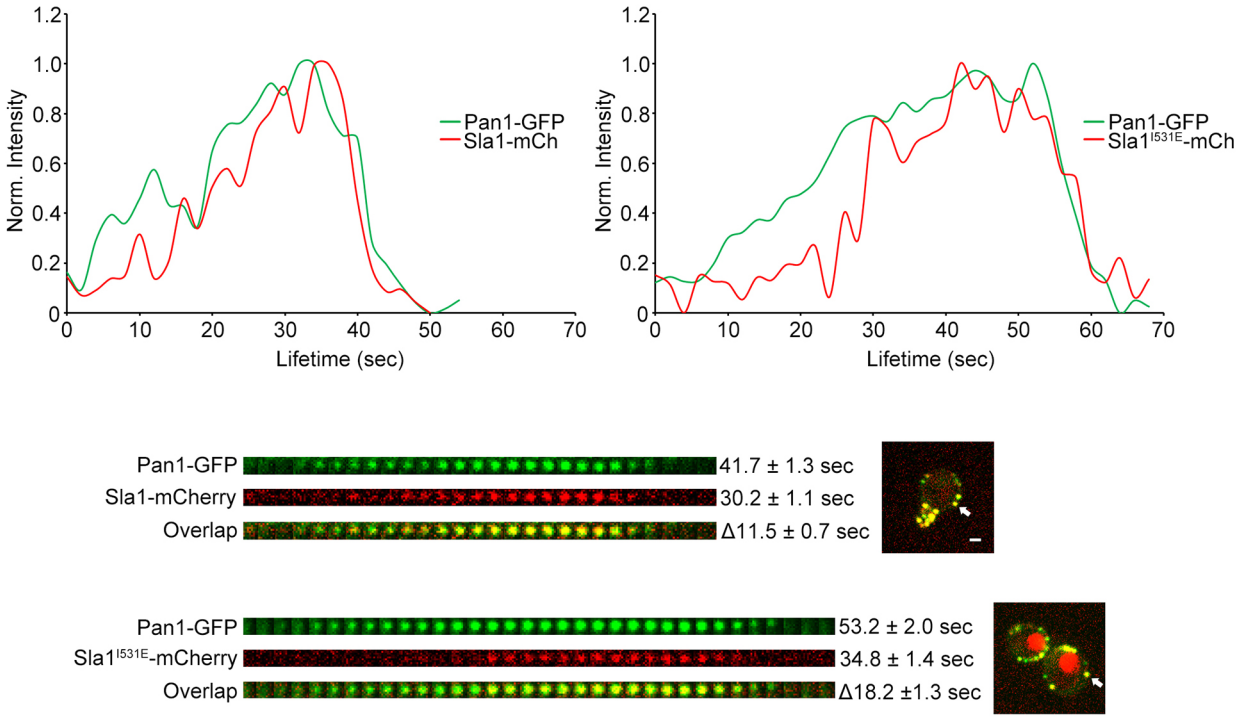

Fig. 8. The Sla1–NPFxD interaction is necessary for normal progression of endocytosis. Cells expressing Sla1^{I531E}–mCherry and Pan1–GFP from the endogenous *SLA1* and *PAN1* loci (SDY814), respectively, and corresponding wild-type Sla1–mCherry cells (SDY802) were subjected to live-cell fluorescence microscopy analysis. The patch lifetime of Pan1–GFP in cells expressing Sla1^{I531E}–mCherry was prolonged compared with that of cells expressing wild-type Sla1–mCherry (n=95 cells, P<0.0001) suggesting a defect in endocytic progression. Graphs (top) show representative examples. Kymographs represent the endocytic patches indicated by arrows in the images (bottom). Values for patch lifetime and the time between arrival of Pan1–GFP and Sla1–mCherry or Sla1^{I531E}–mCherry (Δ) are shown as mean±s.e.m. of n=40 patches. Arrows indicate the patches shown in kymographs. Scale bar: 1 µm.

Henry et al., 2012; Kelly et al., 2014; Kadlecova et al., 2017). This is a difficult question to address *in vivo* given the multitude of cargos and endocytic machinery components that co-exist at a CME site and the possibility for redundancies in the system (Keyel et al., 2006). Furthermore, a number of technical aspects often complicate the analysis. For example, simple adaptor gene deletions are not adequate to address this point, given the numerous interactions adaptor proteins make in addition to binding cargo. Here, we took advantage of the great abundance of knowledge regarding Sla1 and the budding yeast system, which facilitates the study of native components *in vivo*. Our data suggest that binding to cargo containing the NPFxD endocytic signal, and likely also ubiquitylated cargo, contributes to plasma membrane recruitment of the adaptor protein Sla1. Although this requirement is not absolute, the data show that binding to cargo is important for adaptor recruitment. This conclusion is consistent with and extends results obtained using other adaptors and endocytic signals in mammalian systems (Mettlen et al., 2010; Henry et al., 2012).

Previous work demonstrated that the SR region is key for Sla1 function and recruitment to endocytic sites through interactions with Pan1 and End3 (Tang et al., 2000; Chi et al., 2012; Sun et al., 2015). Remarkably, Sla1ΔSR–GFP broadly coats the plasma membrane and does not appear to be internalized with the endocytic vesicle (Chi et al., 2012). Results obtained here indicate that binding to cargo and Pan1 and/or End3 cooperate in Sla1 recruitment. This was most dramatically demonstrated by Sla1^{F507L}ΔSR–GFP and Sla1^{I531E}ΔSR–GFP, which were essentially lost from endocytic sites and the plasma membrane in general. We propose a model in which cargo binding contributes to general recruitment of Sla1 to the plasma membrane, and Pan1 and/or End3 binding mediates recruitment of Sla1 specifically at endocytic sites.

Interestingly, Sla1 interactions with cargo and Pan1 and/or End3 may be coordinated. We found that the Sla1 C-terminal NPFGF-COOH sequence (adjacent to SR) has the ability to bind to SHD1, thus preventing interaction with the NPFxD endocytic signal. It is possible that cytosolic Sla1 adopts a ‘closed’ conformation in which SHD1 and SR are not accessible to interact with NPFxD and Pan1 and/or End3. In fact, Sla1 has been proposed to exist in a ‘closed’ conformation in the cytosol, where the SR region is phosphorylated and unable to interact with Pan1 and/or End3 (Chi et al., 2012). Dephosphorylation of the SR region, mediated by PP1–Scd5, would then ‘open up’ Sla1 allowing interaction with Pan1 and/or End3 (Chi et al., 2012). An attractive model is that such ‘open’ Sla1 conformation would simultaneously allow binding to Pan1 and/or End3, as well as cargo containing the NPFxD signal. This model would explain why Sla1ΔSR–GFP broadly coats the plasma membrane, because SHD1 would be always available to bind plasma membrane proteins containing the NPFxD signal (no negative regulation by the C-terminal NPFGF-COOH sequence). This model would also help explain why Sla1–GFP remains largely cytosolic in cells carrying truncations of the Pan1 and End3 regions that interact with Sla1 (Sun et al., 2015). In addition to dephosphorylation of the SR region, stabilization of the ‘open’ Sla1 conformation likely requires binding to Pan1 and/or End3. Thus, in the absence of interaction with Pan1 and/or End3, the Sla1 C-terminal NPFGF-COOH sequence may remain bound to SHD1 and inhibit membrane recruitment regardless of phosphorylation status.

The contribution of the C-terminal NPFGF-COOH sequence to Sla1 function appears to be complex. The reduction of Sla1ΔNPFGF–GFP plasma membrane levels suggests that the Sla1 C-terminal NPFGF-COOH sequence may have additional functions besides inhibiting the interaction between SHD1 and

cargo containing the NPFXD endocytic signal. Such additional functions could have a positive effect on Sla1 recruitment. For example, in the 'open' Sla1 conformation the NPFGF-COOH sequence could bind to CME components containing the EH domain, which is known to bind to NPF motifs. Further studies are necessary to fully understand the function of the C-terminal NPFGF-COOH sequence.

Multiple interactions with cargo might be needed for optimal recruitment of Sla1 to the plasma membrane. This could be accomplished through simultaneous binding of NPFxD-containing and ubiquitylated plasma membrane proteins via the SHD1 and SH3(3) domains, respectively. Sla1 also has the ability to oligomerize via SHD2–SHD2 interactions, thus bringing multiple SHD1 and SH3(3) domains together and enhancing the ability to bind multiple cargo molecules (Di Pietro et al., 2010). Such SHD2–SHD2 interaction is believed to be coupled to the release of the Sla1 variable clathrin box and therefore occur concomitantly with clathrin binding at endocytic sites (Di Pietro et al., 2010). This mechanism would help link cargo binding with recruitment to endocytic sites and reinforce the coordination of interactions that Sla1 in an 'open' conformation would make with cargo and coat, as discussed above for Pan1 and/or End3.

Ubiquitin-mediated endocytosis is a major mechanism by which plasma membrane proteins are internalized in yeast (Terrell et al., 1998). Yet, strains carrying deletions of the ubiquitin binding motifs of Ede1 and Ent1/Ent2 are still able to internalize ubiquitylated cargo (Dores et al., 2010). The discovery that the Sla1 SH3(3) domain can bind ubiquitin *in vitro* raised the possibility that Sla1 could serve as an adaptor for ubiquitylated cargo *in vivo* (Stamenova et al., 2007). The data presented here suggest that SH3(3) can bind ubiquitylated plasma membrane proteins *in vivo* and contribute to the recruitment of Sla1. Hence, Sla1 probably works as an adaptor for the internalization of ubiquitylated membrane proteins in cooperation with Ede1 and Ent1/Ent2. This is a complex issue to address because, in addition to potential adaptor redundancy, the endocytic machinery itself is subject to regulation by ubiquitylation and deubiquitylation (Weinberg and Drubin, 2014). More work needs to be done to clearly establish Sla1 as an adaptor for ubiquitylated cargo and to reveal any interplay with Ede1 and Ent1/Ent2. This should be an area of important future research.

Internalization of integral membrane cargo proteins is a central function of CME. Accordingly, it is reasonable to propose that the endocytic machinery might have the ability to sense cargo load. Data from budding yeast supports this idea. For example, the early arriving endocytic machinery protein Ede1 has a shorter patch lifetime in the bud, where polarized secretion is expected to provide more cargo than in the mother cell (Layton et al., 2011). Secretory mutant strains appear to be delayed in transitioning from early to late stages of endocytosis, but there is a partial recovery when cargo load is increased by triggering endocytosis of the amino acid permease Gap1 (Carroll et al., 2012). The relatively subtle delay in progression of endocytosis observed here in terms of Pan1–GFP patch lifetime in *sla1*^{I531E} cells is consistent with NPFxD-cargo load having a role regulating endocytosis progression, but is not consistent with a switch-like checkpoint.

MATERIALS AND METHODS

Plasmids

High-copy plasmids encoding *SLA1* and various truncations and mutations were generated using PCR amplification and In-Fusion cloning (Takara Bio). A plasmid (pSDP894) was generated based on pGBT9 (Clontech) in which the sequence encoding for the GAL4 DNA binding domain was replaced with the sequence encoding Sla1 amino acids 495–560, corresponding to the SHD1 domain. The sequence encoding for GFP was subsequently cloned in frame following SHD1 to generate pSDP904 (SHD1–GFP and Frag 5–GFP). The fragment encoding SHD1 in pSDP904 was subsequently replaced with one encoding full-length Sla1 to generate pSDP965 (Sla1–GFP). pSDP964 (Frag 1–GFP) was generated by replacing SHD1 in pSDP904 with Sla1 amino acids 1–560. pSDP963 (Frag 2–GFP) was generated by replacing SHD1 in pSDP904 with Sla1 amino acids 120–560, which span the region immediately after SH3(2), SH3(3) and SHD1. pSDP962 (Frag 3–GFP) was generated by replacing SHD1 in pSDP904 with Sla1 amino acids 350–560, corresponding to SH3(3) and SHD1. pSDP978 [SH3(3)–GFP and Frag 4–GFP] was generated by replacing SHD1 in pSDP904 with Sla1 amino acids 350–420 corresponding to SH3(3). pSDP979 (Frag 3^{W391A}–GFP) was generated by introducing point mutation W391A into pSDP962. pSDP997 (Frag 3–NPFGF–GFP) was generated by introducing a fragment encoding Sla1 residues 1214–1244 between Sla1 residue 560 and GFP in pSDP962. pSDP1054 (Frag 3^{I531E}–GFP) was generated by introducing point mutation I531E into pSDP962. A plasmid to visualize the nuclear pore complex (pBJ090: Nup133–3×mCherry::URA3) was donated by Steven Markus (Department of Biochemistry and Molecular Biology, Colorado State University, Fort Collins, CO).

Plasmids encoding for two and three repeats of the Sla1 SHD1 or SH3(3) domains were generated using PCR amplification and In-Fusion cloning. pSDP1059 (2×SHD1–GFP) was generated by insertion of a fragment encoding for a second SHD1 domain (amino acids 495–560) into pSDP904. pSDP1061 (3×SHD1–GFP) was generated by insertion of a third SHD1 domain into pSDP1059. pSDP1060 [2×SH3(3)–GFP] was generated by insertion of a fragment encoding for a second SH3(3) domain (amino acids 350–420) into pSDP978. pSDP1062 [3×SH3(3)–GFP] was generated by insertion of a third SH3(3) domain into pSDP1060.

Plasmids encoding for recombinant GST–3×NPFSD and GST–3×NPASD have been described previously (Mahadev et al., 2007). Plasmids encoding for recombinant polyhistidine-tagged versions of SHD1 (pSDP1134), SHD1^{I531E} (pSDP1135), SHD1–NPFGF (pSDP1136), and SHD1–NPAGF (pSDP1137) were generated by In-Fusion cloning into pET30a(+) (Novagen).

Yeast strains

GPY4914 (*MATα ura3-52, leu2, 112 his3-Δ200, trp1Δ901, lys2-801, suc2-Δ9 GAL-MEL SLA1-GFP::TRP1*) (Di Pietro et al., 2010) was crossed with SDY1032 (*MATa ura3-52, leu2, 112 his3-Δ200, trp1Δ901, lys2-801, suc2-Δ9 GAL-MEL PAN1-RFP::HIS3*) and the resultant diploid was subjected to sporulation and tetrad dissection to generate SDY1422 (*MATα ura3-52, leu2, 112 his3-Δ200, trp1Δ901, lys2-801, suc2-Δ9 GAL-MEL SLA1-GFP::TRP, PAN1-RFP::HIS3*). Strains carrying the SHD1 point mutations in the endogenous *SLA1* gene were previously generated (Mahadev et al., 2007). Here, to allow for fluorescence microscopy imaging, standard methods (Ito et al., 1983; Sikorski and Hieter, 1989) were utilized to add a C-terminal GFP sequence, thus generating SDY542 (*MATa ura3-52, leu2-3, 112 his3-Δ200, trp1-Δ901, lys2-801, suc2-Δ9 sst1::LYS2, Ste2::Leu, sla1*^{I531E}*-GFP::TRP*), SDY545 (*MATa ura3-52, leu2-3, 112 his3-Δ200, trp1-Δ901, lys2-801, suc2-Δ9 sst1::LYS2, Ste2::Leu, sla1*^{F507L}*-GFP::TRP*), SDY546 (*MATa ura3-52, leu2-3, 112 his3-Δ200, trp1-Δ901, lys2-801, suc2-Δ9 sst1::LYS2, Ste2::Leu, sla1*^{K525A}*-GFP::TRP*). These strains were then crossed with SEY6210 (*MATα ura3-52, leu2, 112 his3-Δ200, trp1Δ901, lys2-801, suc2-Δ9 GAL-MEL*) (Robinson et al., 1988) and the resultant diploids were subject to sporulation and tetrad dissection to generate SDY1423 (*MATα ura3-52, leu2-3, 112 his3-Δ200, trp1-Δ901, lys2-801, suc2-Δ9, sla1*^{I531E}*-GFP::TRP*), SDY1424 (*MATα ura3-52, leu2-3, 112 his3-Δ200, trp1-Δ901, lys2-801, suc2-Δ9, sla1*^{F507L}*-GFP::TRP*) and SDY1426 (*MATα ura3-52, leu2-3, 112 his3-Δ200, trp1-Δ901, lys2-801, suc2-Δ9, sla1*^{K525A}*-GFP::TRP*). These strains were then crossed with SDY1032 (*MATa ura3-52, leu2, 112 his3-Δ200, trp1Δ901, lys2-801, suc2-Δ9 GAL-MEL PAN1-RFP::HIS3*) and the resultant diploids were subject to sporulation and tetrad dissection to generate SDY599 (*MATα ura3-52, leu2-3, 112 his3-Δ200, trp1-Δ901, lys2-801, suc2-Δ9, sla1*^{I531E}*-GFP::TRP, PAN1-RFP::HIS3*), SDY601 (*MATα ura3-52, leu2-3, 112 his3-Δ200, trp1-*

Δ901, lys2-801, suc2-Δ9, sla1^{F507L}-GFP::TRP, PAN1-RFP::HIS3) and SDY603 (*MATα ura3-52, leu2-3, 112 his3-Δ200, trp1-Δ901, lys2-801, suc2-Δ9, sla1^{K525A}-GFP::TRP, PAN1-RFP::HIS3*).

Standard methods were utilized to generate SDY712 (*MATα ura3-52, leu2-3, 112 his3-Δ200, trp1-Δ901, lys2-801, suc2-Δ9 GAL, sla1ΔSR-GFP::TRP*) from SEY6210 (Robinson et al., 1988). SDY718 (*MATa ura3-52, leu2-3, 112 his3-Δ200, trp1-Δ901, lys2-801, suc2-Δ9 sst1::LYS2, Ste2::Leu, sla1^{I531E}ΔSR-GFP::TRP*), SDY736 (*MATa ura3-52, leu2-3, 112 his3-Δ200, trp1-Δ901, lys2-801, suc2-Δ9 sst1::LYS2, Ste2::Leu, sla1^{F507L}ΔSR-GFP::TRP*), SDY738 (*MATa ura3-52, leu2-3, 112 his3-Δ200, trp1-Δ901, lys2-801, suc2-Δ9 sst1::LYS2, Ste2::Leu, sla1^{K525A}ΔSR-GFP::TRP*) were generated from strains harboring the corresponding point mutations in the full-length endogenous *SLA1* gene using standard methods (Ito et al., 1983; Sikorski and Hieter, 1989; Mahadev et al., 2007). The same standard methods were utilized to generate SDY783 (*MATa ura3-52, leu2-3, 112 his3-Δ200, trp1-Δ901, lys2-801, suc2-Δ9 GAL, STE2-GFP::TRP*) from SEY6211. SDY712 (*MATα ura3-52, leu2-3, 112 his3-Δ200, trp1-Δ901, lys2-801, suc2-Δ9 GAL, sla1ΔSR-GFP::TRP*) was crossed with SDY795 (*MATa ura3-52, leu2-3, 112 his3-Δ200, trp1-Δ901, lys2-801, suc2-Δ9 GAL, PAN1-mCherry::HIS*) and the resultant diploid was subjected to sporulation and tetrad dissection to generate SDY913 (*MATα ura3-52, leu2-3, 112 his3-Δ200, trp1-Δ901, lys2-801, suc2-Δ9 GAL, sla1ΔSR-GFP::TRP, PAN1-mCherry::HIS*).

Mutation to the Sla1 SH3-3 domain was introduced into the endogenous *SLA1* gene in SEY6210 (*MATα ura3-52, leu2, 112 his3-Δ200, trp1Δ901, lys2-801, suc2-Δ9 GAL-MEL*) using a two-step approach similar to those described previously (Mahadev et al., 2007; Di Pietro et al., 2010). First, a PCR-amplified *URA3* product containing flanking *SLA1* sequences corresponding to regions upstream of SH3(3) and downstream of the LLDLQ clathrin-binding sequence (nucleotides 959–2458) were transformed into SEY6210 to generate SDY739, in which the fragment spanning from SH3(3) to LLDLQ was replaced by *URA3*. Second, these cells were co-transformed with an *SLA1* fragment containing the W391A point mutation and a pRS313 (*HIS3*). His+ colonies were then replica-plated onto 5-fluorotic acid plates to identify cells that contained the W391A mutant sequence replacing *URA3*, thus resulting in generation of SDY818 (*MATα ura3-52, leu2, 112 his3-Δ200, trp1Δ901, lys2-801, suc2-Δ9 GAL-MEL sla1^{W391A}*). Standard methods were then applied to SDY818 in order to generate SDY832 (*MATα ura3-52, leu2-3, 112 his3-Δ200, trp1-Δ901, lys2-801, suc2-Δ9 GAL, sla1^{W391A}-GFP::TRP*). Standard methods were utilized to generate SDY802 (*MATα ura3-52, leu2, 112 his3-Δ200, trp1Δ901, lys2-801, suc2-Δ9 GAL-MEL SLA1-mCherry::HIS3, Pan1-GFP::TRP1*), SDY814 (*MATa ura3-52, leu2-3, 112 his3-Δ200, trp1-Δ901, lys2-801, suc2-Δ9 sst1::LYS2, sla1^{I531E}-mCherry::HIS3, Pan1-GFP::TRP1*), SDY1486 (*MATa ura3-52, leu2-3, 112 his3-Δ200, trp1-Δ901, lys2-801, suc2-Δ9 sst1::LYS2, Ste2::Leu, sla1ΔNPFGF-GFP::TRP*), and SDY1488 (*MATa ura3-52, leu2-3, 112 his3-Δ200, trp1-Δ901, lys2-801, suc2-Δ9 sst1::LYS2, Ste2::Leu, sla1^{F507L}ΔNPFGF-GFP::TRP*).

Strains presented in Fig. S1 were generated by transformation of plasmid pBJ090 into yeast strains GPY4914, SDY542, SDY545 and SDY546 to generate yeast strains SDY704 (*MATα ura3-52, leu2, 112 his3-Δ200, trp1Δ901, lys2-801, suc2-Δ9 GAL-MEL SLA1-GFP::TRP1*, Nup133–3×mCherry::URA3), SDY705 (*MATa ura3-52, leu2-3, 112 his3-Δ200, trp1-Δ901, lys2-801, suc2-Δ9 sst1::LYS2, Ste2::Leu, sla1^{I531E}-GFP::TRP*, Nup133–3×mCherry::URA3), SDY706 (*MATa ura3-52, leu2-3, 112 his3-Δ200, trp1-Δ901, lys2-801, suc2-Δ9 sst1::LYS2, Ste2::Leu, sla1^{F507L}-GFP::TRP*, Nup133–3×mCherry::URA3), SDY707 (*MATa ura3-52, leu2-3, 112 his3-Δ200, trp1-Δ901, lys2-801, suc2-Δ9 sst1::LYS2, Ste2::Leu, sla1^{K525A}-GFP::TRP*, Nup133–3×mCherry::URA3). Control immunoblotting analysis of total cell extracts using antibodies against Sla1 (gift from Dr Gregory Payne, Department of Biological Chemistry, University of California at Los Angeles School of Medicine, CA; used in a 1:1000 dilution) indicated that the expression level and stability of various mutants was indistinguishable from wild-type Sla1–GFP.

Fluorescence microscopy

Fluorescence microscopy imaging was performed, as described previously (Feliciano et al., 2011), using an Olympus IX81 spinning-disk confocal microscope with a Photometrics Cascade II camera and a 100×/1.40 numerical aperture objective. Cells were grown to early log phase and single-plane images or movies were acquired at room temperature. Imaging software Slidebook 6 (3I, Denver, CO) was used for capturing and analysis. In Figs 1 and 6, Sla1–GFP peak patch:cytosol ratio was determined by drawing a mask on individual endocytic sites, to measure the average fluorescence intensity for that area, and a second mask that measured the average fluorescence intensity of the cytosolic region (avoiding the nucleus and vacuole, which become readily apparent upon increasing the contrast). The two fluorescence intensity values were recorded for the movie frame in which the endocytic patch fluorescence intensity was at its maximum. The peak patch:cytosol ratio was then calculated by dividing the two fluorescence intensity values. In Figs 1, 2, 4–8, the total-membrane:cytosol ratio was determined in randomly acquired single plane frames by first drawing a mask around the entire plasma membrane of the cell and measuring the average fluorescence intensity for the masked area. A second mask was then drawn in the cytosolic region (avoiding the nucleus and vacuole), and the average fluorescence was measured. The total-membrane:cytosol ratio was then calculated by dividing the two fluorescence intensity values. In Fig. 3A, a mask was drawn covering the plasma membrane on the region subjected to photobleaching, and the average fluorescence intensity was measured for each frame of the movie. Values were normalized to the fluorescence intensity before photobleaching. In Fig. 8 (upper panels), the fluorescence intensity of endocytic patches at each time point was normalized to that of the maximum patch intensity. In Fig. S2, nuclear:cytosol fluorescence intensity ratio was measured by drawing a mask in the region encompassed by Nup133–3×mCherry and a second mask outside the Nup133–3×mCherry region.

Biochemical methods

GST and polyhistidine fusion proteins were expressed in *E. coli* (BL21) and purified as previously described (Di Pietro et al., 2004; Mahadev et al., 2007). GST pulldown experiments were performed as described previously (Bultema et al., 2012; Feliciano et al., 2015). Briefly, GST fusion proteins (50 µg) were bound to glutathione–Sepharose beads (40 µl) for 1 h, followed by three washes to remove unbound GST fusion proteins, addition of the polyhistidine fusion proteins (20 µg) in phosphate-buffered saline (PBS) (1 ml total volume), and incubation at 4°C for 90 min while rotating. Beads were then washed three times with PBS containing 0.2% Triton X-100 and once with PBS. Bound proteins were analyzed by SDS–PAGE. Loading controls for each polyhistidine fusion protein were also carried out by SDS–PAGE to verify equal amounts of protein were used during the experiment. Total yeast cell extracts were generated from early log cultures (5 A_{500} unit equivalents/ml) by glass bead lysis (Ferro-Novick et al., 1984). Immunoblotting analysis of total cell extracts was performed as described previously (Ambrosio et al., 2012).

Statistical analysis

Error bars indicate mean±s.e.m. Statistical significance between samples was determined using unpaired Student's *t*-tests (GraphPad Prism Software, La Jolla, CA): **P*<0.05, ***P*<0.01, ****P*<0.001, *****P*<0.0001.

Acknowledgements

We thank Steven Markus for the generous gift of plasmid pBJ090 and Andrea Ambrosio for help with figure preparation. The microscope used in this work is supported in part by the CSU Microscope Imaging Network core infrastructure grant.

Competing interests

The authors declare no competing or financial interests.

Author contributions

Conceptualization: T.O.T., S.M.D.P.; Methodology: T.O.T., H.P.F., D.M.O.; Validation: T.O.T.; Formal analysis: T.O.T., H.P.F., S.M.D.P.; Investigation: T.O.T., H.P.F., D.M.O.; Data curation: T.O.T., H.P.F., S.M.D.P.; Writing - original draft: T.O.T.; Writing - review & editing: T.O.T., S.M.D.P.; Visualization: T.O.T., S.M.D.P.; Supervision: S.M.D.P.; Project administration: S.M.D.P.; Funding acquisition: S.M.D.P.

Funding

This work was supported by National Science Foundation grant MCB-1616775 and National Institutes of Health grant GM-125619 to S.M.D.P. An American Heart

Association predoctoral fellowship provided support to T.O.T. Deposited in PMC for release after 12 months.

Supplementary information

Supplementary information available online at
https://jcs.biologists.org/lookup/doi/10.1242/jcs.247684.supplemental

Peer review history

The peer review history is available online at
https://jcs.biologists.org/lookup/doi/10.1242/jcs.247684.reviewer-comments.pdf

References

Aguet, F., Antonescu, C. N., Mettlen, M., Schmid, S. L. and Danuser, G. (2013). Advances in analysis of low signal-to-noise images link dynamin and AP2 to the functions of an endocytic checkpoint. *Dev. Cell* **26**, 279-291. doi:10.1016/j.devcel.2013.06.019

Aguilar, R. C., Watson, H. A. and Wendland, B. (2003). The yeast Epsin Ent1 is recruited to membranes through multiple independent interactions. *J. Biol. Chem.* **278**, 10737-10743. doi:10.1074/jbc.M211622200

Ambrosio, A. L., Boyle, J. A. and Di Pietro, S. M. (2012). Mechanism of platelet dense granule biogenesis: study of cargo transport and function of Rab32 and Rab38 in a model system. *Blood* **120**, 4072-4081. doi:10.1182/blood-2012-04-420745

Apel, A. R., Hoban, K., Chuartzman, S., Tonikian, R., Sidhu, S., Schuldiner, M., Wendland, B. and Prosser, D. (2017). Syp1 regulates the clathrin-mediated and clathrin-independent endocytosis of multiple cargo proteins through a novel sorting motif. *Mol. Biol. Cell* **28**, 2434-2448. doi:10.1091/mbc.e15-10-0731

Avinoam, O., Schorb, M., Beese, C. J., Briggs, J. A. and Kaksonen, M. (2015). ENDOCYTOSIS. Endocytic sites mature by continuous bending and remodeling of the clathrin coat. *Science* **348**, 1369-1372.

Boettner, D. R., Chi, R. J. and Lemmon, S. K. (2012). Lessons from yeast for clathrin-mediated endocytosis. *Nat. Cell Biol.* **14**, 2-10. doi:10.1038/ncb2403

Bultema, J. J., Ambrosio, A. L., Burek, C. L. and Di Pietro, S. M. (2012). BLOC-2, AP-3, and AP-1 proteins function in concert with Rab38 and Rab32 proteins to mediate protein trafficking to lysosome-related organelles. *J. Biol. Chem.* **287**, 19550-19563. doi:10.1074/jbc.M112.351908

Carroll, S. Y., Stimpson, H. E., Weinberg, J., Toret, C. P., Sun, Y. and Drubin, D. G. (2012). Analysis of yeast endocytic site formation and maturation through a regulatory transition point. *Mol. Biol. Cell* **23**, 657-668. doi:10.1091/mbc.e11-02-0108

Chapa-y-Lazo, B., Allwood, E. G., Smaczynska-de Rooij, I. I., Snape, M. L. and Ayscough, K. R. (2014). Yeast endocytic adaptor AP-2 binds the stress sensor Mid2 and functions in polarized cell responses. *Traffic* **15**, 546-557. doi:10.1111/tra.12155

Chi, R. J., Torres, O. T., Segarra, V. A., Lansley, T., Chang, J. S., Newpher, T. M. and Lemmon, S. K. et al. (2012). Role of Scd5, a protein phosphatase-1 targeting protein, in phosphoregulation of Sla1 during endocytosis. *J. Cell Sci.* **125**, 4728-4739. doi:10.1242/jcs.098871

Di Pietro, S. M., Falcón-Pérez, J. M. and Dell'Angelica, E. C. (2004). Characterization of BLOC-2, a complex containing the Hermansky-Pudlak syndrome proteins HPS3, HPS5 and HPS6. *Traffic* **5**, 276-283. doi:10.1111/j.1600-0854.2004.0171.x

Di Pietro, S. M., Cascio, D., Feliciano, D., Bowie, J. U. and Payne, G. S. (2010). Regulation of clathrin adaptor function in endocytosis: novel role for the SAM domain. *EMBO J.* **29**, 1033-1044. doi:10.1038/emboj.2010.5

Dores, M. R., Schnell, J. D., Maldonado-Baez, L., Wendland, B. and Hicke, L. (2010). The function of yeast epsin and Ede1 ubiquitin-binding domains during receptor internalization. *Traffic* **11**, 151-160. doi:10.1111/j.1600-0854.2009.01003.x

Feliciano, D. and Di Pietro, S. M. (2012). SLAC, a complex between Sla1 and Las17, regulates actin polymerization during clathrin-mediated endocytosis. *Mol. Biol. Cell* **23**, 4256-4272. doi:10.1091/mbc.e11-12-1022

Feliciano, D., Bultema, J. J., Ambrosio, A. L. and Di Pietro, S. M. (2011). In vivo andin vitro studies of adaptor-clathrin interaction. *J. Vis. Exp*.

Feliciano, D., Tolsma, T. O., Farrell, K. B., Aradi, A. and Di Pietro, S. M. (2015). A second Las17 monomeric actin-binding motif functions in Arp2/3-dependent actin polymerization during endocytosis. *Traffic* **16**, 379-397. doi:10.1111/tra.12259

Ferro-Novick, S., Novick, P., Field, C. and Schekman, R. (1984). Yeast secretory mutants that block the formation of active cell surface enzymes. *J. Cell Biol.* **98**, 35-43. doi:10.1083/jcb.98.1.35

Gardiner, F. C., Costa, R. and Ayscough, K. R. (2007). Nucleocytoplasmic trafficking is required for functioning of the adaptor protein Sla1p in endocytosis. *Traffic* **8**, 347-358. doi:10.1111/j.1600-0854.2007.00534.x

Goode, B. L., Eskin, J. A. and Wendland, B. (2015). Actin and endocytosis in budding yeast. *Genetics* **199**, 315-358. doi:10.1534/genetics.112.145540

Henry, A. G., Hislop, J. N., Grove, J., Thorn, K., Marsh, M. and von Zastrow, M. (2012). Regulation of endocytic clathrin dynamics by cargo ubiquitination. *Dev. Cell* **23**, 519-532. doi:10.1016/j.devcel.2012.08.003

Holtzman, D. A., Yang, S. and Drubin, D. G. (1993). Synthetic-lethal interactions identify two novel genes, SLA1 and SLA2, that control membrane cytoskeleton assembly in Saccharomyces cerevisiae. *J. Cell Biol.* **122**, 635-644. doi:10.1083/jcb.122.3.635

Howard, J. P., Hutton, J. L., Olson, J. M. and Payne, G. S. (2002). Sla1p serves as the targeting signal recognition factor for NPFX(1,2)D-mediated endocytosis. *J. Cell Biol.* **157**, 315-326. doi:10.1083/jcb.200110027

Ito, H., Fukuda, Y., Murata, , K. and Kimura, , A. (1983). Transformation of intact yeast cells treated with alkali cations. *J. Bacteriol.* **153**, 163-168. doi:10.1128/JB.153.1.163-168.1983

Kadlecova, Z., Spielman, S. J., Loerke, D., Mohanakrishnan, A., Reed, D. K. and Schmid, S. (2017). Regulation of clathrin-mediated endocytosis by hierarchical allosteric activation of AP2. *J. Cell Biol.* **216**, 167-179. doi:10.1083/jcb.201608071

Kelly, B. T., Graham, S. C., Liska, N., Dannhauser, P. N., Honing, S., Ungewickell, E. J. and Owen, D. J. (2014). Clathrin adaptors. AP2 controls clathrin polymerization with a membrane-activated switch. *Science* **345**, 459-463. doi:10.1126/science.1254836

Keyel, P. A., Mishra, S. K., Roth, R., Heuser, J. E., Watkins, S. C. and Traub, L. M. (2006). A single common portal for clathrin-mediated endocytosis of distinct cargo governed by cargo-selective adaptors. *Mol. Biol. Cell* **17**, 4300-4317. doi:10.1091/mbc.e06-05-0421

Kirchhausen, T. (1999). Adaptors for clathrin-mediated traffic. *Annu. Rev. Cell Dev. Biol.* **15**, 705-732. doi:10.1146/annurev.cellbio.15.1.705

Kukulski, W., Schorb, M., Kaksonen, M. and Briggs, J. A. (2012). Plasma membrane reshaping during endocytosis is revealed by time-resolved electron tomography. *Cell* **150**, 508-520. doi:10.1016/j.cell.2012.05.046

Layton, A. T., Savage, N. S., Howell, A. S., Carroll, S. Y., Drubin, D. G. and Lew, D. J. (2011). Modeling vesicle traffic reveals unexpected consequences for Cdc42p-mediated polarity establishment. *Curr. Biol.* **21**, 184-194. doi:10.1016/j.cub.2011.01.012

Lemmon, S. K. and Traub, L. M. (2012). Getting in touch with the clathrin terminal domain. *Traffic* **13**, 511-519. doi:10.1111/j.1600-0854.2011.01321.x

Liu, K., Hua, Z., Nepute, J. A. and Graham, T. R. (2007). Yeast P4-ATPases Drs2p and Dnf1p are essential cargos of the NPFXD/Sla1p endocytic pathway. *Mol. Biol. Cell* **18**, 487-500. doi:10.1091/mbc.e06-07-0592

Loerke, D., Mettlen, M., Yarar, D., Jaqaman, K., Jaqaman, H., Danuser, G. and Schmid, S. L. (2009). Cargo and dynamin regulate clathrin-coated pit maturation. *PLoS Biol.* **7**, e57. doi:10.1371/journal.pbio.1000057

Mahadev, R. K., Di Pietro, S. M., Olson, J. M., Piao, H. L., Payne, G. S. and Overduin, M. (2007). Structure of Sla1p homology domain 1 and interaction with the NPFxD endocytic internalization motif. *EMBO J.* **26**, 1963-1971. doi:10.1038/sj.emboj.7601646

McMahon, H. T. and Boucrot, E. (2011). Molecular mechanism and physiological functions of clathrin-mediated endocytosis. *Nat. Rev. Mol. Cell Biol.* **12**, 517-533. doi:10.1038/nrm3151

Mettlen, M., Loerke, D., Yarar, D., Danuser, G. and Schmid, S. L. (2010). Cargo- and adaptor-specific mechanisms regulate clathrin-mediated endocytosis. *J. Cell Biol.* **188**, 919-933. doi:10.1083/jcb.200908078

Owen, D. J., Collins, B. M. and Evans, P. R. (2004). Adaptors for clathrin coats: structure and function. *Annu. Rev. Cell Dev. Biol.* **20**, 153-191. doi:10.1146/annurev.cellbio.20.010403.104543

Piao, H. L., Machado, I. M. and Payne, G. S. (2007). NPFXD-mediated endocytosis is required for polarity and function of a yeast cell wall stress sensor. *Mol. Biol. Cell* **18**, 57-65. doi:10.1091/mbc.e06-08-0721

Puthenveedu, M. A. and von Zastrow, M. (2006). Cargo regulates clathrin-coated pit dynamics. *Cell* **127**, 113-124. doi:10.1016/j.cell.2006.08.035

Reider, A. and Wendland, B. (2011). Endocytic adaptors-social networking at the plasma membrane. *J. Cell Sci.* **124**, 1613-1622. doi:10.1242/jcs.073395

Reider, A., Barker, S. L., Mishra, S. K., Im, Y. J., Maldonado-Báez, L., Hurley, J. H., Traub, L. M. and Wendland, B. (2009). Syp1 is a conserved endocytic adaptor that contains domains involved in cargo selection and membrane tubulation. *EMBO J.* **28**, 3103-3116. doi:10.1038/emboj.2009.248

Robinson, J. S., Klionsky, D. J., Banta, L. M. and Emr, S. D. (1988). Protein sorting in Saccharomyces cerevisiae: isolation of mutants defective in the delivery and processing of multiple vacuolar hydrolases. *Mol. Cell. Biol.* **8**, 4936-4948. doi:10.1128/MCB.8.11.4936

Rodal, A. A., Manning, A. L., Goode, B. L. and Drubin, D. G. (2003). Negative regulation of yeast WASp by two SH3 domain-containing proteins. *Curr. Biol.* **13**, 1000-1008. doi:10.1016/S0960-9822(03)00383-X

Sikorski, R. S. and Hieter, P. (1989). A system of shuttle vectors and yeast host strains designed for efficient manipulation of DNA in Saccharomyces cerevisiae. *Genetics* **122**, 19-27.

Stamenova, S. D., French, M. E., He, Y., Francis, S. A., Kramer, Z. B. and Hicke, L. (2007). Ubiquitin binds to and regulates a subset of SH3 domains. *Mol. Cell* **25**, 273-284. doi:10.1016/j.molcel.2006.12.016

Sun, Y., Leong, N. T., Wong, T. and Drubin, D. G. (2015). A Pan1/End3/Sla1 complex links Arp2/3-mediated actin assembly to sites of clathrin-mediated endocytosis. *Mol. Biol. Cell* **26**, 3841-3856. doi:10.1091/mbc.E15-04-0252

Tan, P. K., Howard, J. P. and Payne, G. S. (1996). The sequence NPFXD defines a new class of endocytosis signal in Saccharomyces cerevisiae. *J. Cell Biol.* **135**, 1789-1800. doi:10.1083/jcb.135.6.1789

Tang, H.-Y., Xu, J. and Cai, M. (2000). Pan1p, End3p, and S1a1p, three yeast proteins required for normal cortical actin cytoskeleton organization, associate with each other and play essential roles in cell wall morphogenesis. *Mol. Cell. Biol.* **20**, 12-25. doi:10.1128/MCB.20.1.12-25.2000

Terrell, J., Shih, S., Dunn, R. and Hicke, L. (1998). A function for monoubiquitination in the internalization of a G protein-coupled receptor. *Mol. Cell* **1**, 193-202. doi:10.1016/S1097-2765(00)80020-9

Tolsma, T. O., Cuevas, L. M. and Di Pietro, S. M. (2018). The Sla1 adaptor-clathrin interaction regulates coat formation and progression of endocytosis. *Traffic* **19**, 446-462. doi:10.1111/tra.12563

Toshima, J. Y., Toshima, J., Kaksonen, M., Martin, A. C., King, D. S. and Drubin, D. G. (2006). Spatial dynamics of receptor-mediated endocytic trafficking in budding yeast revealed by using fluorescent alpha-factor derivatives. *Proc. Natl Acad. Sci. USA* **103**, 5793-5798. doi:10.1073/pnas.0601042103

Traub, L. M. and Bonifacino, J. S. (2013). Cargo recognition in clathrin-mediated endocytosis. *Cold Spring Harbor Perspect. Biol.* **5**, a016790. doi:10.1101/cshperspect.a016790

Weinberg, J. and Drubin, D. G. (2012). Clathrin-mediated endocytosis in budding yeast. *Trends Cell Biol.* **22**, 1-13. doi:10.1016/j.tcb.2011.09.001

Weinberg, J. S. and Drubin, D. G. (2014). Regulation of clathrin-mediated endocytosis by dynamic ubiquitination and deubiquitination. *Curr. Biol.* **24**, 951-959. doi:10.1016/j.cub.2014.03.038

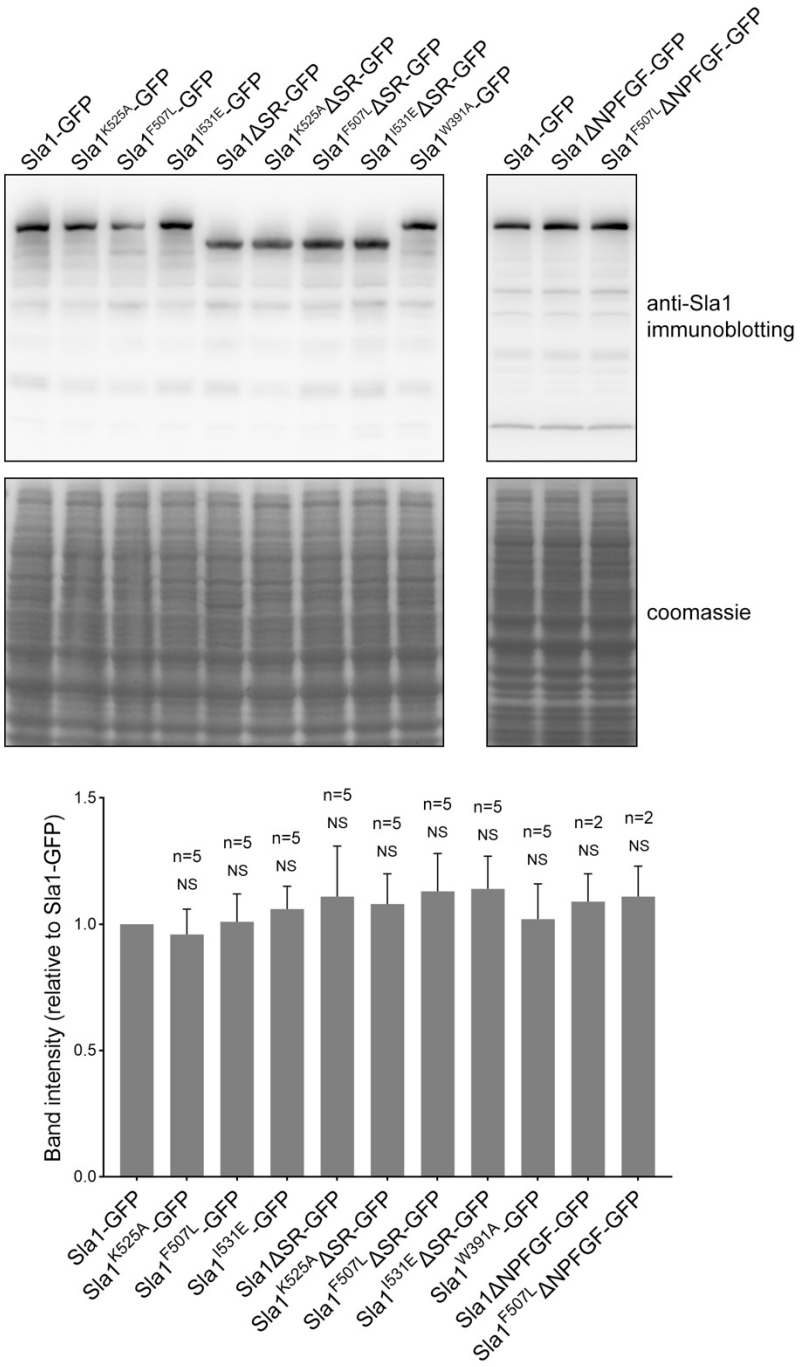

Figure S1. Immunoblotting analysis of strains expressing wild type and mutant forms of Sla1-GFP. Upper panels, total cell extracts were generated from strains expressing Sla1-GFP (SDY1422), Sla1^{K525A}-GFP (SDY603), Sla1^{F507L}-GFP (SDY601), Sla1^{I531E}-GFP (SDY599), Sla1ΔSR-GFP (SDY712), Sla1^{K525A}ΔSR-GFP (SDY738), Sla1^{F507L}ΔSR-GFP (SDY736), Sla1^{I531E}ΔSR-GFP (SDY718), Sla1^{W391A}-GFP (SDY832), Sla1ΔNPFGF-GFP (SDY1486), or Sla1^{F507L}ΔNPFGF-GFP (SDY1488) from the *SLA1* endogenous locus and analyzed by immunoblotting with anti-Sla1 antibodies. Middle panels, loading control. Lower panel, quantification of the band intensity for Sla1-GFP mutants relative to wild type Sla1-GFP (5 biological replicates were analyzed for strains shown in the left panels and 2 biological replicates for strains shown in the right panels). Differences in band intensities relative to wild type Sla1-GFP were not significant (NS).

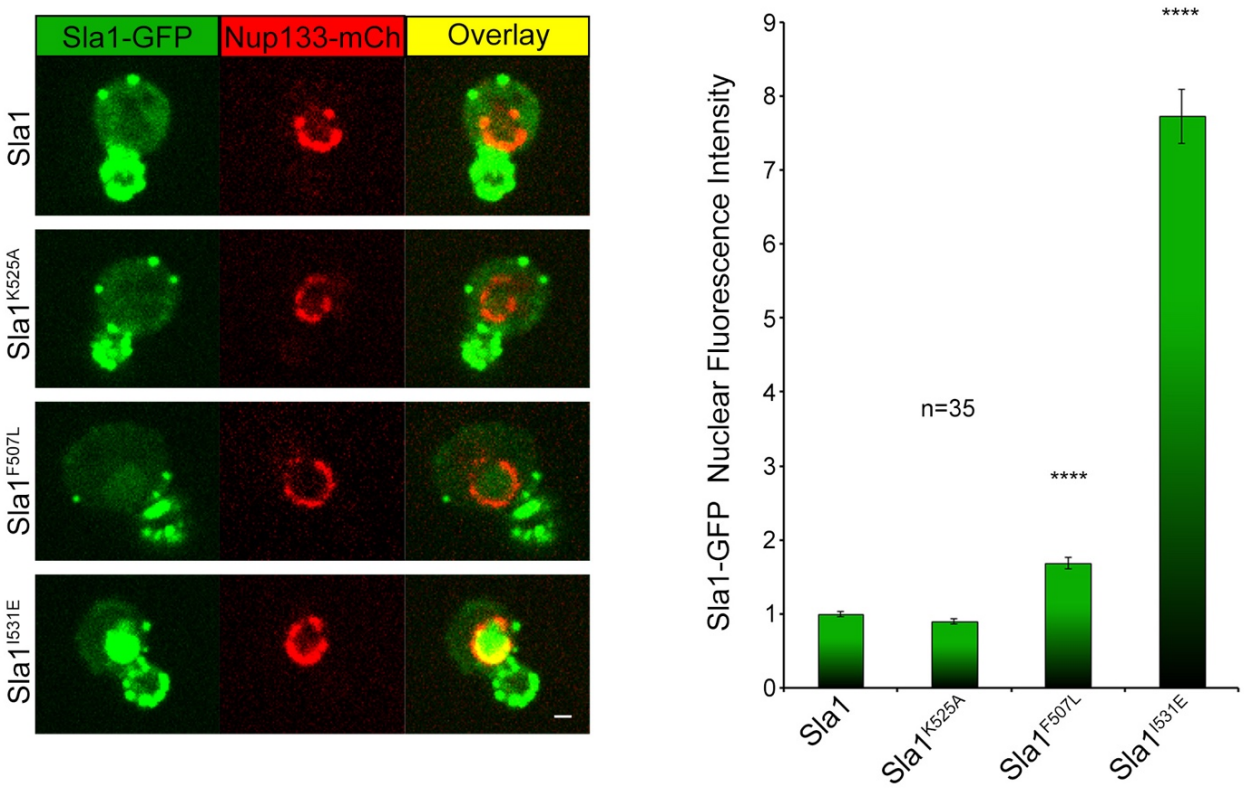

Figure S2. Sla1 localizes to the nucleus when NPFxD binding is disrupted. Live-cell confocal fluorescence microscopy imaging of cells expressing Sla1-GFP wild type, or the indicated SHD1 mutant from the endogenous locus and Nup133-3xmCherry expressed from a plasmid. Left, representative frames of Sla1-GFP and Nup133-3xmCherry in wild type and Sla1 mutant cells. Right, quantification of the Sla1-GFP nuclear/cytoplasm fluorescence intensity ratio showing a significant increase in Sla1-GFP nuclear localization was determined for F507L and I531E mutants (n=35 cells, P=0.0566 for $Sla1^{K525A}$, P<0.0001 for $Sla1^{F507L}$ and $Sla1^{I531E}$). Scale bar = 1 µm.

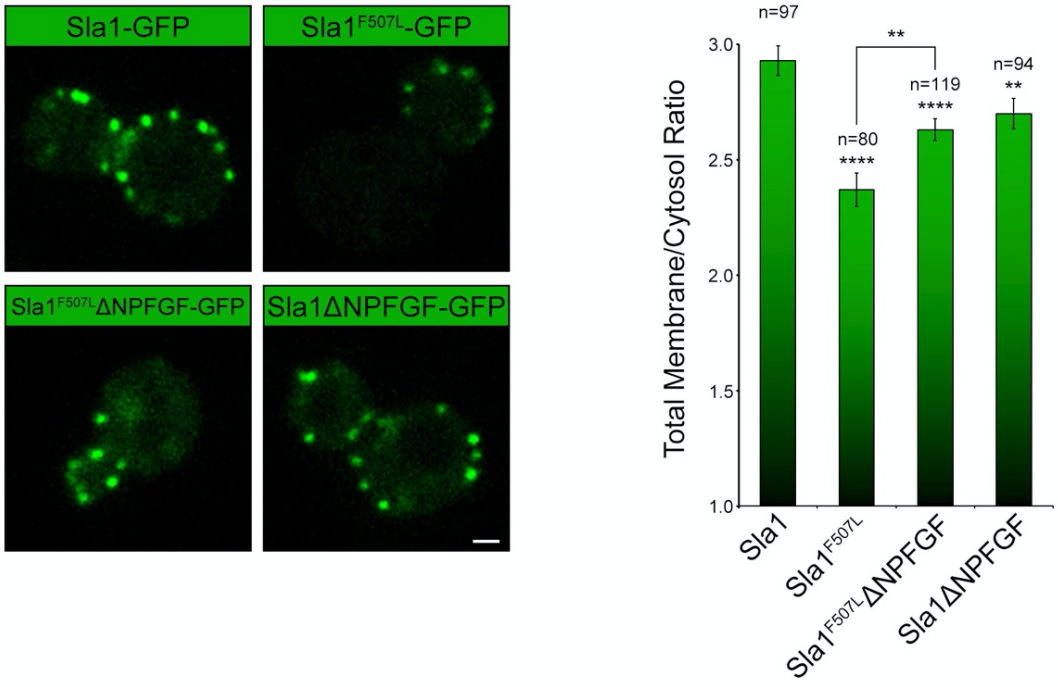

Figure S3. The NPFGF-COOH sequence at the Sla1 C-terminus affects Sla1 recruitment to the plasma membrane. Live-cell confocal fluorescence microscopy analysis of yeast cells expressing either Sla1-GFP (SDY1422), Sla1^{F507L}-GFP (SDY601), Sla1^{F507L}ΔNPFGF-GFP (SDY1488) or Sla1ΔNPFGF-GFP (SDY1486) from the endogenous *SLA1* locus. Left, panels show representative frames from each strain. Right, quantification represented as Total Membrane/Cytosol Ratio of fluorescence intensity across the entire cell plasma membrane was performed as described under Materials and Methods and shows a recruitment defect for Sla1^{F507L}-GFP, Sla1^{F507L}ΔNPFGF-GFP and Sla1ΔNPFGF-GFP relative to Sla1-GFP (n=97 cells for Sla1; n=80 cells, P<0.0001 for Sla1^{F507L}-GFP; n=119, P<0.0001 for Sla1^{F507L}ΔNPFGF-GFP; n=94, P<0.01 for Sla1ΔNPFGF-GFP). Importantly, the plasma membrane levels of Sla1^{F507L}ΔNPFGF-GFP were higher than Sla1^{F507L}-GFP (P<0.01). Scale bar = 1 μm.